Quaternary International 470 (2018) 130–147

Contents lists available at ScienceDirect

Quaternary International

journal homepage: www.elsevier.com/locate/quaint

The role of earthquakes and climate in the formation of diamictic sediments in a New Zealand mountain lake

C.A. Woodward [a, b, *], A. Slee [c], P. Gadd [b], A. Zawadzki [b], H. Hamze [b], A. Parmar [b], D. Zahra [b]

[a] School of Earth & Environmental Sciences, The University of Queensland, Australia
[b] Australian Nuclear Science & Technology Organisation, Lucas Heights, Australia
[c] Forest Practices Authority, 30 Patrick Street, Hobart, Australia

ARTICLE INFO

Article history:
Received 14 August 2017
Received in revised form
24 October 2017
Accepted 31 October 2017
Available online 15 November 2017

Keywords:
New Zealand
Holocene
Mountain lake
Diamicton
Earthquakes
Climate

ABSTRACT

We used Itrax XRF, magnetic susceptibility, grain size, and micro-CT scanning to provide a facies classification for a Late Holocene sediment sequence from Lake Chappa'ai in the Southern Alps, New Zealand. The record contained multiple diamictic layers and our objective was to determine the environmental significance of these deposits. Clast fabric analysis indicated that the diamicts comprise dropstones transported to the centre of the lake by ice rafting. Diamicts belonging to Facies 1 represent rock falls onto lake ice triggered by earthquakes that produced MMI (Modified Mercalli Intensity) > 8 shaking in the catchment. MMI >8 earthquakes may need to occur when the lake has ice cover to produce Facies 1 diamicts. MMI >8 earthquakes in the ice free season or MMI 7–8 earthquakes may also result in an increased flux of large (>1 mm) clasts to the centre of the lake, but may not produce a Facies 1 diamict. More work is required to establish the role of climate related processes on the formation of non-Facies 1 diamicts in Lake Chappa'ai. Climate change may directly lead to diamict formation by changing lake ice cover and facilitating transport of large clasts by anchor ice, or increasing the likelihood of rain on snow events in the spring. Changing ice cover conditions will also affect how mountain lakes record past earthquake events. Lakes that are ice free will not produce earthquake diamicts and lakes that have perennial ice cover may produce a single diamict representing multiple earthquakes if the lake becomes ice free. A reduction in the duration of winter ice cover will also decrease the probability of capturing primary rockfall deposits from earthquakes. Additional data, such as a diatom or chironomid record from Lake Chappa'ai may help to resolve the contribution of climate processes to diamict formation. We should consider the Lake Chappa'ai record as an indicator of minimum earthquake activity until we can disentangle the effects of climate change on non-Facies 1 diamict formation. This study highlights the multiple mechanisms that can lead to diamict formation in mountain lake sediments. These processes should always be considered before attributing the presence of diamict deposits to ice-rafted debris in a pro-glacial lake. This is particularly true in seismically active settings where earthquake triggered rockfalls may lead to diamict formation.

1. Introduction

There have been many studies on mountain lake sediment records in the northern hemisphere, including studies on past climate change (Battarbee et al., 2002; Catalan et al., 2002; Koinig et al., 2002; Lotter et al., 2002), human impacts (Hundey et al., 2014), snow avalanche records (Nesje et al., 2007) and flood histories (Glur et al., 2013). There are only a handful of records from mountain lakes in the Southern Hemisphere, including limited records from South America (Bird et al., 2011; Stansell et al., 2013; Bao et al., 2015; De Jong et al., 2016; Martel-Cea et al., 2016), Africa (Woller et al., 2000), Australia (Stanley and De Deckker, 2002), and New Zealand (Shulmeister et al., 2003; Jara et al., 2015). We therefore know little about how humans have impacted these systems, and we have just started to explore their potential as paleoenvironmental records. We also know little about lake and catchment processes in Southern Hemisphere mountain lakes.

There are many mountain lakes in New Zealand (Fig. 1) and it's geological and climatological setting makes New Zealand an

* Corresponding author. Australian Nuclear Science & Technology Organisation, Lucas Heights, Australia.
E-mail address: craigw@ansto.gov.au (C.A. Woodward).

https://doi.org/10.1016/j.quaint.2017.10.051
1040-6182/

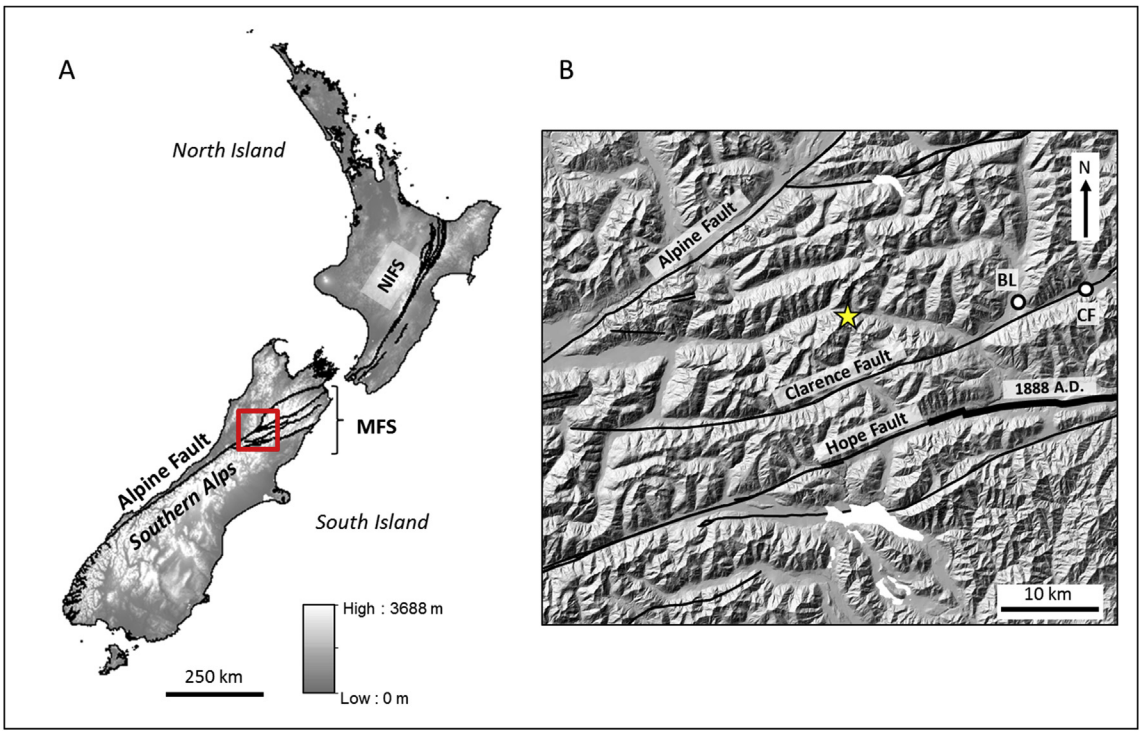

Fig. 1. The location of the study site. A. Digital elevation model (DEM) of New Zealand showing major fault lines. The red square shows the extent of Fig. 1B. MFS = Marlborough Fault System, NIFS = North Island Fault System B. DEM showing the location of the Lake Chappa'ai catchment (yellow star) and major fault lines (black lines). The thick black line on the Hope Fault shows the western limit of the fault rupture associated with the 1888 A.D. Amuri earthquake according to Khajavi et al. (2016). BL = Boyle Lodge climate station. CF = Locality of offset terraces dating the last Clarence Fault earthquake (Knuepfer, 1992). (For interpretation of the references to colour in this figure legend, the reader is referred to the web version of this article.)

excellent location to study climate change and geomorphic processes. New Zealand is tectonically active, mainly due to the collision of the Pacific Plate in the east with the Indo-Australian Plate to the west. This results in uplift rates in the Southern Alps of up to 10 mm per year (Adams, 1980). The predominantly westerly airflow over the Southern Alps (Fig. 1) results in a strong orographic precipitation gradient, with up to 15 m of precipitation falling on the western side each year (Griffiths and McSaveney, 1983). Paleoenvironmental research on New Zealand mountain lakes is limited to surface sediment sampling for transfer function training sets (Woodward and Shulmeister, 2006; Dieffenbacher-Krall et al., 2007), the development of biochemical proxies (Zink et al., 2010) and a limited number of pollen records (Shulmeister et al., 2003; Jara et al., 2015).

In this paper we report the first comprehensive study of the sedimentology of a mountain lake from the South Island, New Zealand (Fig. 1). The sediments from this lake are interesting because they contain frequent diamictic layers. Sediment deposits are classified as diamicts if they comprise a poorly sorted clast-sand-mud mixture (Eyles et al., 1983). Diamicts in lake sediments are significant as they are often used to infer the deposition of ice-rafted debris in pro-glacial lakes (Smith, 2000). Diamicts in lake sediments can also be formed by other processes such as snow avalanches onto lake ice (Luckman, 1975; Nesje et al., 2007), flooding (Fouinat et al., 2017), or adfreezing of littoral lake deposits onto anchor ice (Kempema et al., 2001).

We propose and test multiple hypotheses for the formation of diamictic sediments in a New Zealand mountain lake. The diamictic sediments could represent significant regional changes or stochastic lake and catchment processes. Stochastic processes include the uneven fallout of large clasts during seasonal melting of lake ice and sporadic rockfalls onto lake ice during winter. Rockfalls can be triggered by slope instability caused by freeze-thaw cycles, frost cracking and frost wedging (Matsuoka, 2001). Alternatively, the diamictic sediments could indicate earthquake triggered rock-falls onto lake ice, or the onset of ice-rafting in a proglacial lake. Climate change could also lead to changes in thickness and persistence of ice cover and this could affect the formation of anchor ice and the transport of ice rafted debris (Adrian et al., 2009).

We use multiple techniques (Itrax XRF, magnetic susceptibility, grain size, and micro-CT scanning) to develop a lithofacies classification for sediments from a New Zealand mountain lake. Lithofacies are sediment deposits sharing similar sedimentological characteristics, such as grain size, sedimentary structures and geochemistry (Eyles et al., 1983). We use this lithofacies classification, and comparison to known regional environmental events (e.g. climate change and earthquakes) to identify the most likely cause for the formation of the diamictic sediments. We also compare the stratigraphy from two cores collected from the same lake to test whether the diamicton horizons represent the uneven fall-out of clasts during the break up of seasonal ice cover.

2. Regional setting

Lake Chappa'ai (unofficial name, 42° 31′ 55″ S, 172° 11′, 2″ E) is a small (0.02 km^2) cirque lake at an altitude of 1470 m, with a maximum depth of 6.8 m, a catchment area of 0.15 km^2 and a maximum catchment elevation of 1660 m (Fig. 2). The bedrock comprises strongly indurated greywacke and argillite (metamorphosed sandstone and mudstone) from the Triassic Torlesse Group (Gregg, 1964). The lake catchment is close to three active strike-slip faults; it is 15 km SE from the Alpine fault, 6 km NW from the Clarence Fault and 12 km NW from the Hope fault (Fig. 1). Knowledge of past earthquakes on these faults is derived from

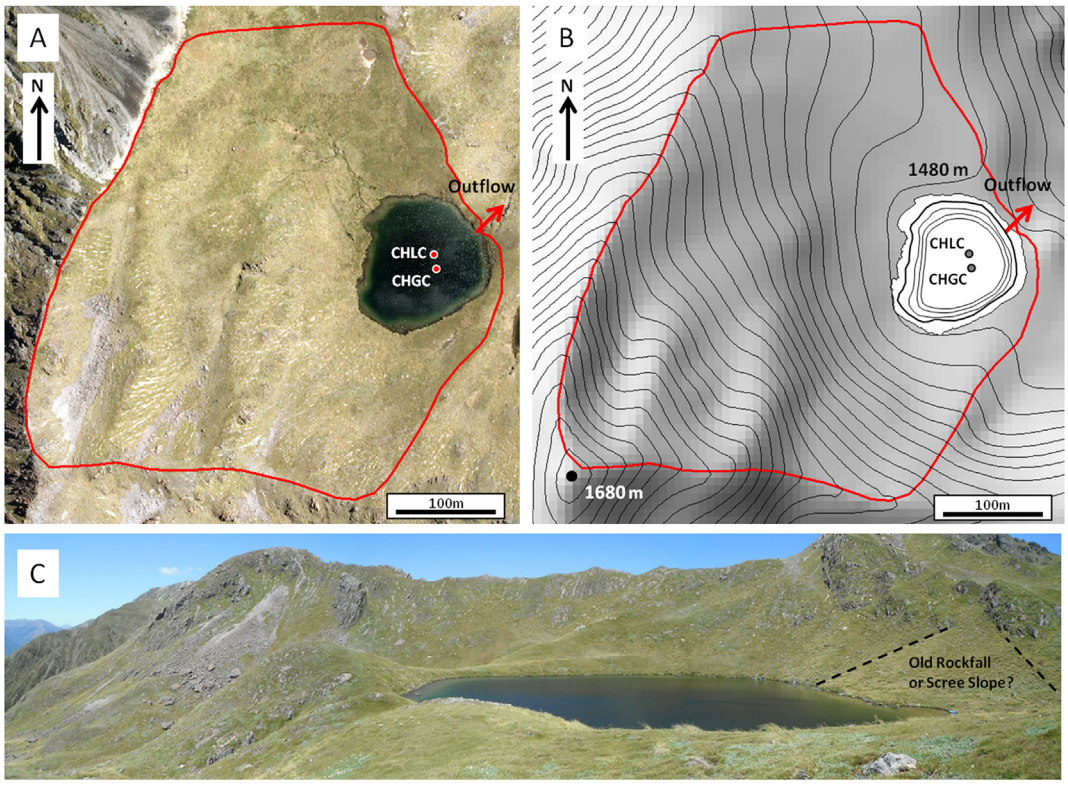

Fig. 2. The Lake Chappa'ai catchment. A and B depict the catchment boundary (red line) superimposed on a satellite image (A) and shaded DEM (B). Topographic contours in B are in intervals of 8 m. The thick black bathymetric contour in B is 1 m depth and light grey contours indicate 2, 4 and 6 m depth intervals. The location of the core site for the long core (CHLC) and short core (CHGC) are indicated in A and B. C. A photograph of the lake catchment looking south. Note the steep terrain to the right of the image (west of the lake) which could be a source of rockfalls. The extent of a possible old rockfall or inactive, vegetated scree surface is indicated with black dashed lines. (For interpretation of the references to colour in this figure legend, the reader is referred to the web version of this article.)

records of paleoseismicity from lake records (Howarth et al., 2014, 2016), dendrochronology (Wells et al., 1999) and by dating changes in stratigraphy in trenches and soil pits spanning fault boundaries (Wells et al., 1999; Langridge et al., 2013; Khajavi et al., 2016). The Clarence and Hope Faults are capable of producing M_W ~ 7 earthquakes, and the Alpine Fault can produce earthquakes of magnitude $M_W \geq 8$ (Howarth et al., 2014, 2016).

The Lake Chappa'ai catchment is several hundred metres above the local altitudinal tree-line which varies between 1000 and 1200 m. The vegetation in the catchment is dominated by narrow-leaved snow tussock (*Chionochloa pallens*) and carpet grass (*Chionochloa australis*) (Fig. 2). There are limited observations on climate in the Southern Alps and no studies on lake-ice phenology (formation and breakup). Climate data for this site must be extrapolated from elsewhere in New Zealand using models and climate surfaces. This information can be supplemented with observations from satellite imagery. Extraction of precipitation data from a climate surface (Leathwick et al., 2002) provides a mean annual precipitation of 3300 mm. Observations from other sites, and modelling (Clark et al., 2009) suggests that > 30% of annual precipitation could fall as snow at this altitude. Monthly mean air temperatures for this site were extrapolated from a temperature record spanning 1985–2017 A.D. from the nearest climate station (Boyle Lodge, Fig. 1) (National Institute for Water and Atmospheric Research, 2017). A lapse rate of 0.6 ± 0.1 °C/100 m (Hales and Roering, 2005) was used to account for the altitudinal difference of 875 m between the study site and the Boyle Lodge climate station. The mean temperature of the coldest month is − 1.6 ± 0.9 °C and the mean temperature for the warmest month (February) is 10 ± 0.9 °C. Seasonal lake-ice cover forms on Northern Hemisphere lakes when the mean air temperature in the coldest month is below 0 °C (Leppäranta, 2015). Calculated monthly average temperatures for June, July and August at this site from 1985 to 2017 were below 0 °C. Satellite imagery from 2002 to 2017 shows ice cover on the lake by the middle of June and ice free conditions by October.

3. Materials and methods

3.1. Core collection

Two cores were collected from Lake Chappa'ai in the summer of 2016. Lake bathymetry was surveyed from an inflatable boat using a Hawkeye depth finder to determine the best coring location. The coring site (Fig. 2) was selected to minimise edge effects and possible slumping of sediments. A 75 cm core (CHLC) was collected from 6.8 m water depth using a Universal Percussion Corer, manufactured by Aquatic Research Instruments. The Universal corer is a portable system that can be used in remote areas to collect cores that are longer than typical gravity cores (i.e. > 50 cm), but still collect an undisturbed sediment-water interface. A 1 m, 68 mm internal diameter core tube was used during percussion coring. The depth of penetration was recorded and compared to the length of the recovered core to determine if any compression or sediment loss due to under-sampling had occurred (Woodward and Sloss, 2013). After collection, the core was stabilised with sodium polyacrylate gel following the protocol outlined in Tomkins et al. (2008).

The Universal Corer without the percussion hammer was used to take a gravity core (CHGC) 5 m away from the coring location of CHLC. CHGC was extruded and sub-sampled at 0.5 cm intervals on the lake shore using an extrusion plate and spatula to scrape

sediment into sample bags. The original purpose of the gravity core was to provide a back-up in case there was a problem with stabilisation and transport of CHLC (e.g. the sediment water interface was lost). This was not required but CHGC provides the opportunity to examine possible variation in sediment deposition in the lake. CHLC was split in the laboratory before further analyses using the Geotek core splitter at the Australian Nuclear Science and Technology Organisation (ANSTO), Lucas Heights, Australia.

3.2. Chronology

The upper sediments from CHLC and CHGC were dated using ^{210}Pb. 14 samples from CHLC and 8 samples from CHGC were analysed to determine ^{210}Pb decay profiles by alpha spectrometry at ANSTO. Age determination was based on either a CIC (constant initial concentration) or CRS (constant rate of supply) model (Appleby, 2001). There were no obvious macrofossil targets available so radiocarbon dating was performed on bulk sediment samples. Seven samples were dated from CHLC and two samples were dated from CHGC. Samples were selected to overlap with the ^{210}Pb profile in CHLC to determine if there is an old carbon effect in this lake. Large clasts were removed from bulk sediment samples before pre-treatment. Samples were pre-treated using an acid - alkali - acid (AAA) protocol before radiocarbon analysis on the ANTARES accelerator at ANSTO. Correction of radiocarbon ages on bulk lake sediments for the old carbon effect followed the protocol outlined in Blaauw et al. (2011). A horizon was selected that contained a "pre-bomb" (pre-1955, Hancock et al., 2011) ^{210}Pb date and a radiocarbon date. The ^{210}Pb date was converted to an equivalent radiocarbon date via reverse calibration using the SHCal13 calibration curve (Hogg et al., 2013). The ^{210}Pb radiocarbon age was subtracted from the ^{14}C age from the same horizon to determine the old carbon effect. The uncertainty of the old carbon effect ($\sigma_{\text{old carbon effect}}$) was based on the uncertainty for the bulk sediment (σ_{bulk}) and the reverse calibrated ^{210}Pb age ($\sigma_{210\text{Pb}}$), ($\sigma^2_{\text{old carbon effect}} = \sigma^2_{\text{bulk}} + \sigma^2_{210\text{Pb}}$). The uncertainty on the corrected radiocarbon was the based on the uncertainty of the old carbon effect and the uncorrected bulk sediment age ($\sigma_{\text{uncorrected 14C age}}$), ($\sigma^2_{\text{corrected 14C age}} = \sigma^2_{\text{old carbon effect}} + \sigma^2_{\text{uncorrected 14C age}}$). Age models for CHLC and CHGC were developed using Bacon version 2.2 (Blaauw and Christen, 2011). ^{210}Pb ages and corrected bulk sediment ^{14}C ages were used in the final models. Radiocarbon ages were calibrated in Bacon using the SHCal13 calibration curve (Hogg et al., 2013).

3.3. Itrax XRF geochemistry

Analyses for XRF elemental profiles, radiographs and magnetic susceptibility on CHLC were performed using the Cox Analytical Itrax core scanner located at ANSTO. Operating conditions for XRF were 55 kV and 30 mA, step size 500 μm and 10 s count time. The X-radiograph settings were 40 kV, 30 mA, an exposure time of 550 ms and a resolution of 200 μm. The Itrax produces an X-radiograph that is only 2 cm wide. A composite image that almost spans the entire core width was produced by scanning three 2 cm wide sections. Magnetic susceptibility measurements were carried out at 5 mm intervals. Data was evaluated using Q-Spec version 8.6.0. Elements with low counts (<100 CPS) and with a low signal to noise ratio were eliminated from further analyses (van der Bilt et al., 2015). A runs test was performed (Agin and Godbole, 1992) to test the signal to noise ratio of elemental data normalised to the inc/coh (incoherent/coherent scattering) ratio. Normalising to the inc/coh ratio corrects for variation in water content throughout the core (Davies et al., 2015).

The inc/coh ratio from the molybdenum tube has been shown to be a useful indicator of organic content in lake sediments (Liu et al., 2013). The inc/coh ratio was calibrated by performing loss on ignition (LOI) on 24 samples from CHLC. We used the LOI protocol outlined in Heiri et al. (2001). Samples were selected to represent the full range of inc/coh values from CHLC and areas with major fluctuations in inc/coh values. Regression of inc/coh vs LOI was performed in the computer program Microsoft Excel (Version 14.0.7177.5000, Microsoft Corporation).

Whirl-pac bags containing 0.5 cm sub-samples from CHGC were X-rayed using the Itrax core scanner in order to determine the presence and relative abundance of large clasts. This step was performed prior to sub-sampling for sieving in order to capture the full assemblage of clasts in each sample. The sediment was scraped into a 2 cm wide strip while still inside the sample bag using a spatula and the sediment and bag was held in place using duct tape. This meant that all of the sediment would be scanned in the 2 cm wide beam of the Itrax x-ray. Sample bags were taped onto a plastic sheet so multiple bags could be scanned in one session (Supplementary Fig. 1, Appendix A). This method created an image composite of multiple X-rays from multiple bags. X-ray images from individual bag samples were cropped from the original image and a composite stack of images was composed to enable visualisation of the stratigraphy of large clasts in CHGC.

3.4. Grain size analysis

3 ml sub-samples from CHLC were prepared for grain size analysis following the protocol outlined in Vaasma (2008). This involved sieving to remove clasts >1 mm, treatment with an 80 °C, 30% peroxide solution to remove organics and an 80 °C, 10% potassium hydroxide solution to remove biogenic silica (diatoms and phytoliths). Samples were dispersed in calgon and grain size analysis performed on a Malvern Mastersizer 2000 laser diffraction particle sizer. The grain size distribution of the <1 mm scale was visualised using a contoured surface plot created in SigmaPlot (Version 10.0, SysStat Software). Statistical analysis of the particle size distributions was performed using the GRADISTAT version 8.0 software package (Blott and Pye, 2001). The size distribution of the >1 mm fraction was determined by dry sieving. The size distribution of the >1 mm clasts was summarized by collating clast counts into grain size categories on the Udden Wentworth Scale (e.g. coarse sand, granules, etc.). 3 ml sub-samples from CHGC were sieved to remove clasts >1 mm. Large clasts in CHGC were not subdivided into grain size sub-categories. CHGC data was only used for the calculation of >1 mm clast fluxes so they could be compared with CHLC fluxes.

3.5. Multivariate facies analysis

Cluster analysis was performed on the sedimentological data to separate the stratigraphy from CHLC into separate facies or sections with distinctive sediment properties. The Itrax data was screened to reduce redundancy by removing variables that were highly correlated ($r^2 > 0.9$). Cluster analysis was performed using Ward's method and the Euclidean (dis)similarity measure in the software package PAST version 2.17c (Hammer et al., 2001). The cluster analysis was not stratigraphically constrained as facies units can occur in multiple sections of the same core. Principal components analysis (PCA) was also performed to determine the sedimentological differences between facies. The PCA was performed in CANOCO version 4.5 (ter Braak and Šmilauer, 2002) with all variables centred and standardised. A PCA biplot was produced in CANOCO version 4.5 using CanoDraw (4.14).

3.6. Micro CT scan

Micro-CT (computed tomography) scanning was used as a non-destructive method to analyse the clast fabric in the lake sediments. The traditional method to perform this analysis involves dissection of the sediments and measurement of clast morphology and orientation by hand (Smith, 2000). This method is destructive and time-consuming.

Core samples had already been split before CT scanning. Core samples were scanned using the CT in the Siemens Inveon multi-modality PET/CT installed with the standard X-ray source (fixed focal spot of 40 μm) and standard CCD detector options at ANSTO. This machine can accommodate 300 mm long samples. The sample was placed on the standard 70 mm wide carbon fibre bed pallet and secured with masking tape. To fit the whole 300 mm sample the CT acquisition required 8 bed positions with a 30% field of view (FOV) overlap at low magnification and the full detector FOV (3072 × 2048 pixels). For each bed position the current and voltage were set to 500 μA and 80 kVp respectively, the detector binning was set to 4, with 180 projections over a 360° rotation. The CT data was reconstructed using Inveon Acquisition Workplace 2.0 software using the Feldcamp reconstruction algorithm, Shepp Logan Filter, no down-sampling, with slight noise reduction and a HU calibration applied. This results in a voxel size of 0.1 mm^3

Raw data from CT scanning was processed using the ImageJ FIJI software platform (Schindelin et al., 2012). The large density difference between the clasts and the lake sediment meant that segmentation (digital separation) of the clasts and host sediment was straight-forward. Segmentation was performed using the threshold adjustment function in FIJI, and multiple stack slices were checked for quality control. 3D analysis in FIJI was used to determine the clast fabric following the criteria defined by Domack and Lawson (1985) and Smith (2000). This includes the orientation (azimuth and plunge) of all clasts with an a:b axial ratio >1.5. We included all clasts with a long axis length >1 mm. Eigen values for clast fabric and a stereoplot of clast axis orientation were generated in Stereonet version 9.9.5 (Allmendinger et al., 2012; Cardozo and Allmendinger, 2013). Tests for random distribution of clast azimuths (Rayleigh's R, Rao's U and Chi^2) were performed in PAST version 2.17c (Hammer et al., 2001).

3.7. Estimating local ground shaking due to past earthquakes

Earthquake triggered rockfalls in the catchment could lead to diamict formation. We therefore produced isoseismal ellipses for modified Mercalli intensity (MMI) for earthquakes in the GeoNet New Zealand Earthquake Catalogue (New Zealand Earthquake commission, 2017; GNS Science, 2017) and selected prehistoric earthquakes. In this paper we use the term historic to refer the earthquake record based on documented observations of earthquake phenomena since 1840 A.D. in the GeoNet New Zealand Earthquake Catalogue (New Zealand Earthquake commission, 2017; GNS Science, 2017). We use the term prehistoric to refer to earthquakes where the location and magnitude is estimated based on lake records (Howarth et al., 2014, 2016), dendrochronology (Wells et al., 1999) and by dating changes in stratigraphy in trenches and soil pits spanning fault boundaries (Wells et al., 1999; Langridge et al., 2013).

We used the empirical relationship between distance and energy attenuation of Dowrick and Rhoades (2005) to generate isoseismals. Maximum magnitudes for prehistoric earthquakes were based on the calculations of Cox et al. (2012). Earthquake epicentres were used as the source of earthquake energy for the historic record since information on rupture length is not always available. We compared the timing of historic earthquakes to the ages of diamict layers to see if there was a pattern in the representation of earthquake events. We speculated that there might be a minimum MMI threshold that could produce rockfalls and earthquakes might produce different diamicts if they occurred when the lake was ice free. Ice rafting could be necessary for diamict formation and it is possible that only winter earthquakes are represented.

The results of this analysis were used to guide our selection of prehistoric earthquakes for isoseismal modelling. It is not practical to produce isoseismals for all earthquakes and it is only necessary to do it for earthquakes that produce sufficient shaking for rockfalls in the catchment. We therefore selected all prehistoric earthquakes that could produce MMI >8. This decision was made because this appeared to be the minimum shaking required to produce unequivocal earthquake derived facies (Facies 1). This included earthquakes on the Alpine, Clarence and Hope Faults (Fig. 1). Earthquake histories and potential rupture lengths of faults were based on studies by Howarth et al. (2014, 2016) and Khajavi et al. (2016).

4. Results

4.1. Core stratigraphy

4.1.1. Visual stratigraphy

A 75 cm core was obtained using the universal corer (CHLC) and a 30 cm core was obtained using the gravity corer (CHGC) (Fig. 3). There was complete sediment recovery for the long core so there was not any compression or under sampling during the coring process. The sediment for CHLC and CHGC mainly comprised light brown fine-grained sediment with some darker brown horizons. The most obvious change in CHLC was the presence of a sandy unit between 30 and 40 cm. Some large clasts (>1 mm) were visible after splitting of CHLC. The full extent of variations in sediment composition was revealed by Itrax X-radiographs, XRF and grain size analysis.

4.1.2. Stratigraphy from Itrax X-radiographs

The Itrax X-radiographs from CHGC revealed the presence of two main diamicton horizons (Figs. 3 and 4). Diamicton units comprised coarse sand, granules and pebbles. Large clasts (pebbles) were most abundant from 7.5 to 11.5 cm, and 18–23 cm. Occasional clasts were also present between 2 and 7.5 cm, and below 22 cm. X-radiographs of CHLC revealed five main diamicton horizons (Fig. 3). These occur between 3 and 6 cm, 9–14.5 cm, 18–22 cm, 30–40 cm and ca. 48–57 cm. Coarse sand was also visible between 22 and 42 cm. The diamicton unit between 30 and 40 cm comprised smaller clasts (mostly coarse sand and granules) in a sandy matrix. The other diamicton units were in a less dense, finer silty matrix.

4.2. Chronology

4.2.1. Lead-210

^{210}Pb age models are presented in Supplementary Fig. 2 and 3, Appendix A. The ^{210}Pb decay profile from CHLC was non-monotonic, so the CRS model was accepted for this core (Appleby, 2001). The main deviation from a non-monotonic decay curve occurred above 2 cm in CHLC and probably represents accelerated deposition at this site. The ^{210}Pb decay profile from CHGC was monotonic, so the CIC model was accepted (Appleby, 2001). ^{210}Pb background (~1860 AD) was reached at 11.5 cm in CHLC and 10 cm in CHGC.

4.2.2. Radiocarbon

Radiocarbon dating results are presented in Supplementary Table 1, Appendix A. Uncalibrated radiocarbon ages ranged from

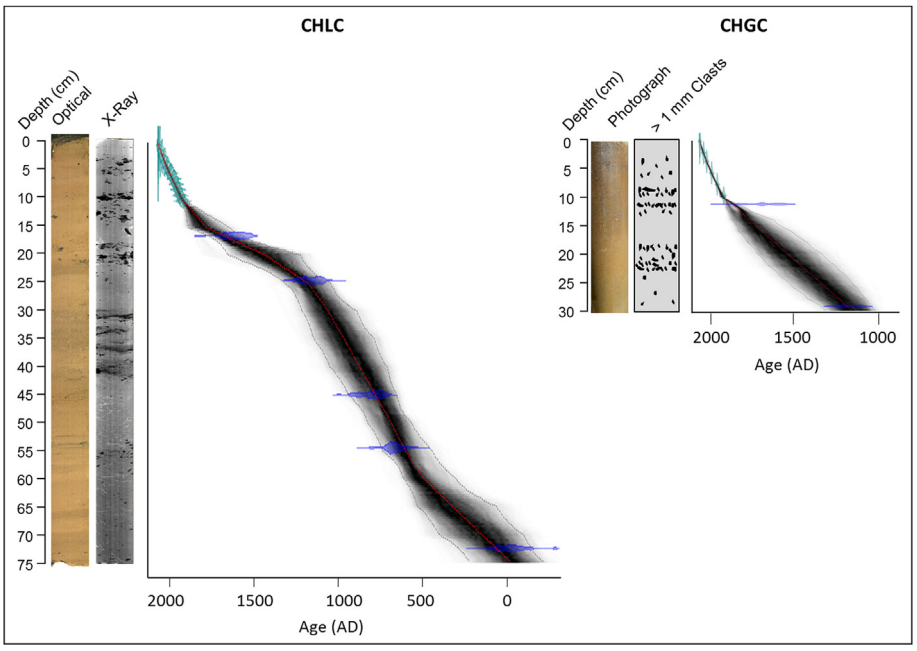

Fig. 3. Stratigraphy and age-depth models for CHLC and CHGC. An optical and X-radiograph image depicts the stratigraphy from CHLC. A photograph of the extruded core taken in the field and a graphical representation of >1 mm clast stratigraphy is used to depict the stratigraphy from CHGC. The age model for CHLC is based on 14 ^{210}Pb and 7 radiocarbon analyses, while the age model for CHGC is based on 6 ^{210}Pb and 2 radiocarbon analyses. See Supplementary Fig. 1 and 2 and Supplementary Table 1 for more information on ^{210}Pb and radiocarbon results.

2930 ± 25 yrs BP to modern in CHLC and 1775 ± 25 to 1135 ± 25 yrs BP in CHGC. Two ages (OZU748 and OZU749) are from the same horizons as ^{210}Pb dates in CHLC. OZU749 coincides with pre-1955 AD deposition, as indicated by the ^{210}Pb. OZU749 is dated to 965 ± 30 yrs BP. The ^{210}Pb date from this horizon yielded an equivalent radiocarbon age of 120 ± 20 BP after reverse calibration. An old carbon effect of 840 ± 40 yrs BP was calculated from the difference between the bulk sediment and radiocarbon reverse calibrated ^{210}Pb age. This old carbon effect was used as an estimate effect of old carbon on bulk sediment radiocarbon dates down core in CHLC and CHGC. Age models constructed using ^{210}Pb and calibrated corrected bulk sediment ages are depicted in Fig. 3.

4.3. Itrax XRF and magnetic susceptibility

The Itrax XRF produced results for 37 variables including 36 elements and the inc/coh ratio. Nineteen elements (Al, As, Au, Bi, Br, Ce, Cl, Cu, In, La, Nb, Nd, P, Pb, Pr, S, Se, Tm, V and Y) were excluded from further analyses as they had counts lower than 100 CPS and/or random distributions. Seventeen variables remained and these were: Ba, Ca, Cr, Dy, Er, Fe, inc/coh, K, Mn, Ni, Rb, Si, Sr, Tb, Ti, Zn, and Zr. The inc/coh ratio was calibrated using loss on ignition measurements so inc/coh could be expressed in terms of organic content. The inc/coh ratio and LOI were highly correlated ($r^2 = 0.7$, $p < 0.001$, $n = 24$). Three samples were excluded from the final calibration model. Two samples were removed as the inc/coh values underestimated typical organic content for a horizon because the XRF beam hit a clast on the sediment surface. One other sample was removed as the LOI underestimated the typical organic content for a horizon because a large clast was sampled. The correlation between the inc/coh ratio and LOI was improved after the removal of the outliers ($r^2 = 0.8$, $p < 0.001$, $n = 21$). Inc/Coh is expressed as LOI in the PCA results.

A PCA plot of the remaining 17 variables (Ba, Ca, Cr, Dy, Er, Fe, LOI, K, Mn, Ni, Rb, Si, Sr, Tb, Ti, Zn, Zr) is provided in Supplementary Fig. 4, Appendix A. PCA axis 1 explained 51.7% of the variation, while PCA axis 2 explained 9.9% of the variation. All variables except for Er, Ni, Dy and Cr highly correlated to PCA axis 1. K, Ca, Ti, Mn, Fe, Zn, Rb, Zr, and Tb were highly correlated ($r^2 > 0.9$). These elements represent a detrital component as these are all elements that are common in the local bedrock (Roser and Korsch, 1999). Fe was retained as a proxy for the detrital component as it had the highest counts (≤32900 CPS). Plots of magnetic susceptibility, Fe, and the calibrated inc/coh ratio data are provided in Fig. 5.

4.4. Grain size

4.4.1. Grains ≤ 1 mm

A contour plot of grain size distributions for the ≤1 mm grain size fraction is depicted in Fig. 6. This is supplemented with plots of individual variables describing changes in grain size, sorting, kurtosis and skewness in Fig. 5. Representative plots of grain size distributions for different parts of the core are also presented in Fig. 7. The examples in Fig. 7 are sourced from separate facies units which will be mentioned later. However, these figures also serve to illustrate changes in the grain size distribution throughout the core. The grain size distributions are frequently bimodal, with a coarser mode ranging from 10 to 150 μm (fine silt to fine sand) and a finer sub-micron (clay) mode. Bimodal distributions are absent between 12 and 22 cm. There are two major shifts in the mean and grain size and the grain size of the dominant mode (Mode 1). Grain size increases at ca. 42 cm then decreases above 20 cm. The grain size of Mode 1 is lowest above 15 cm.

4.4.2. Grains >1 mm

The size distribution of >1 mm clasts in CHLC is depicted in Fig. 6. Clasts >1 mm in CHLC range in size from very coarse sand (1–2 mm) to coarse pebbles (16–32 mm). Clasts are angular and composed of argillite or greywacke (metamorphosed sandstone). No striations were observed on any of the clasts. The upper

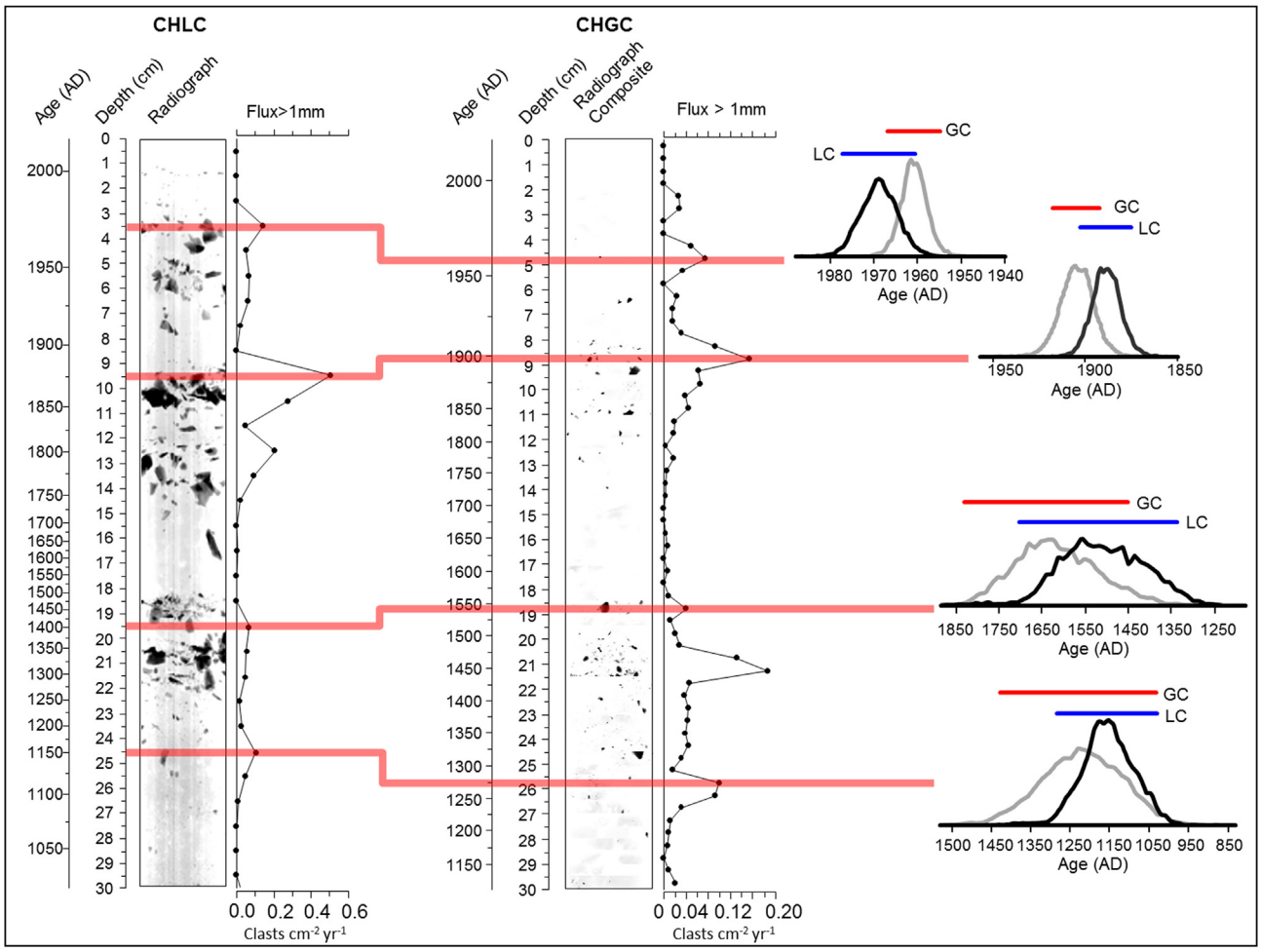

Fig. 4. Comparison of CHLC and CHGC >1 mm clast stratigraphies. X-radiographs from an intact core and individual sample bags are used to depict >1 mm clast stratigraphies the top 30 cm of CHLC and all of CHGC respectively. Contrast and brightness was adjusted to accentuate the clasts. Note that the clasts in the CHGC image are not to scale. The image was composed using individual X-ray images of sediment in sample bags which were 2 cm by 5 cm in area. Each image was cropped and scaled to produce the composite to enable visualisation of clast stratigraphy. The flux of clasts >1 mm in each core is also depicted. Red lines connect common changes in clast flux in both of the cores. These are peaks in clast concentration, or the top of diamicton horizons. Probability density functions (PDFs) extracted from the age models in Fig. 3 are depicted for each of these events. The red and blue horizontal lines depict the 95% confidence interval for CHGC and CHLC respectively. 95% confidence intervals overlap for all of these events. (For interpretation of the references to colour in this figure legend, the reader is referred to the web version of this article.)

diamicton horizons in CHLC tend to contain larger clasts with higher concentrations of fine and medium pebbles. >1 mm clast flux stratigraphies for CHLC and CHGC are depicted in Fig. 4. There are many similarities between the >1 mm clast flux stratigraphies between the two cores. Posterior age probability distributions were extracted from ^{210}Pb and radiocarbon age models for prominent fluctuations in the >1 mm clast flux in both cores. All age probability plots (Fig. 4) indicate that these fluctuations are effectively synchronous in both cores. There are notable peaks in >1 mm flux that don't occur in both cores, including the peak at 12.5 cm in CHLC and the peak at 21.25 cm in CHGC.

4.5. Facies analysis

The results of the cluster analysis to determine sediment facies in CHLC is depicted in Fig. 7. Cluster analysis identified eight major facies in CHLC. Mean values for all variables used in the classification are presented in Supplementary Table 2 in Appendix A. A plot of the stratigraphy of CHLC is depicted in Fig. 7 showing the distribution of the eight major facies in the core and grain size distributions for each facies. The results from the PCA of the 30 variables used in the cluster analysis are shown in Fig. 8. Species scores for PCA axis 1 and PCA axis 2 are provided in Supplementary Table 3. Cluster analysis and the PCA show a major separation in sediment composition between facies 1–5 (Facies Group I) and 6–7 (Facies Group II) (Figs. 7 and 8). The separation of Facies Group I and II occurs along PCA axis 1. PCA axis 1 is primarily a grainsize, organic content and detrital element gradient. Mean grainsize, modal grainsize, the abundance of medium and fine sand have the highest positive PCA axis 1 scores, while organic content (LOI), coarse silt, medium silt and fine silt have the most negative PCA axis 1 scores. PCA axis 2 primarily represents the abundance of clasts >1 mm. The abundance of fine pebbles, granules and very coarse sand have the highest PCA axis 2 scores. Facies Group I samples are spread mostly along PCA axis 2 with a tendency for Facies 1–3 samples to have higher PCA axis 2 scores and Facies 4 and 5 to have lower PCA axis 2 scores.

4.6. Micro CT scan

Processed images of representative diamicts from Facies Group I (0–30 cm) and Facies Group II (30–42 cm) are depicted in Fig. 9.

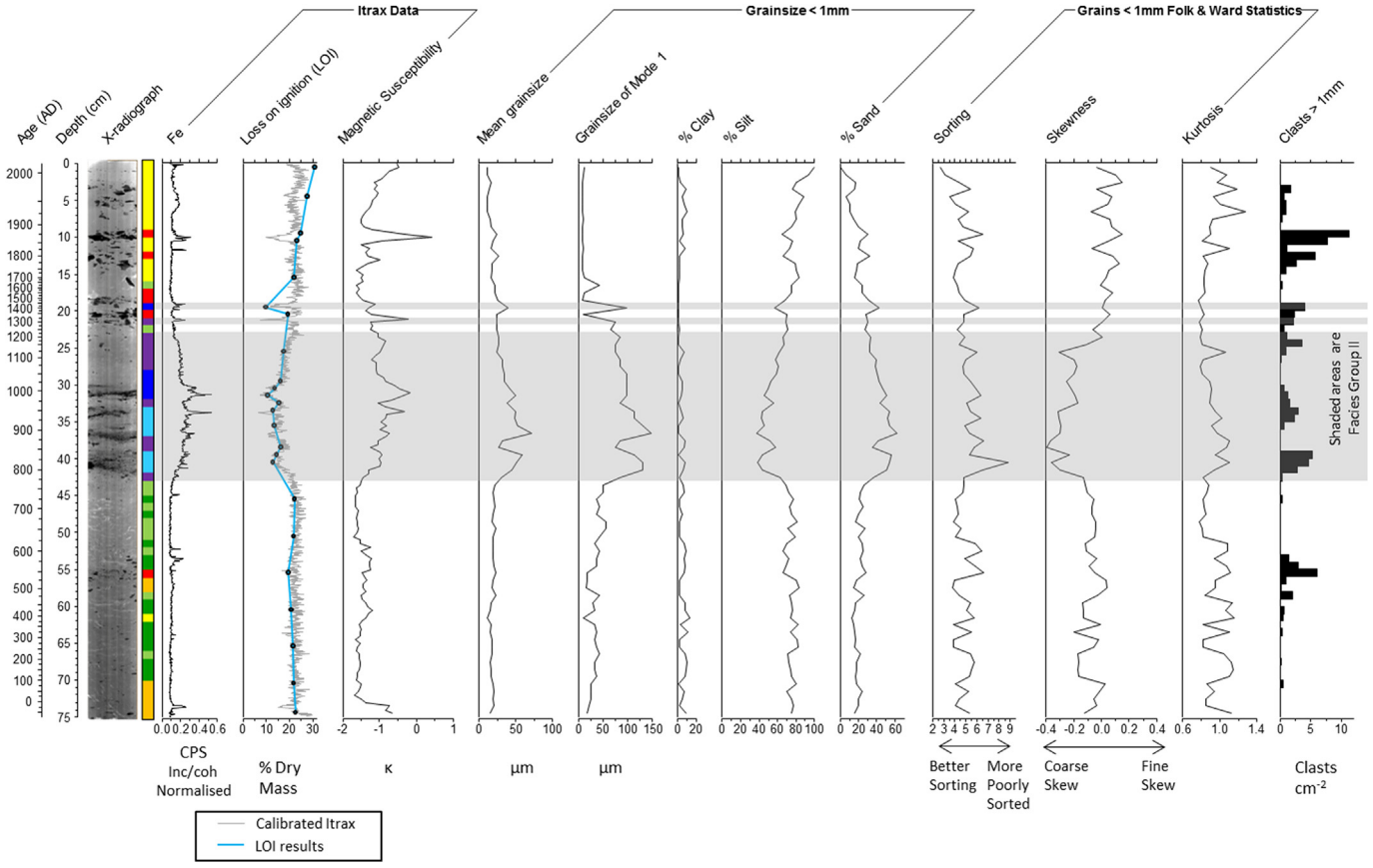

Fig. 5. Stratigraphic plot of Itrax XRF, magnetic susceptibility, organic content and grain size analysis results from CHLC. The results of the lithofacies analysis (Figs. 7 and 8) are also shown beside the X-radiograph. The results of the organic content analysis by loss on ignition (LOI 550, blue line and black circles) are superimposed over calibrated molybdenum incoherent/coherent results. Note the major difference in %Sand, LOI, Fe, skewness, mean and modal grain size between Facies Group I (red, orange, yellow, green bands) and Facies Group II (blue and purple bands, shaded area). (For interpretation of the references to colour in this figure legend, the reader is referred to the web version of this article.)

These images clearly show that the diamicton clasts in Facies Group I tend to be tightly clustered. Many of the clasts that are lower in the sediment than the main diamict layer are located near the edge of the core barrel or on the sliced surface. Diamicton clasts in Facies Group II are not tightly clustered. The CT image Facies Group II diamicts also clearly illustrates the lower average particle size of the clasts.

A total of 492 clasts with a long axis > 1 mm and a:b axial ratio >1.5 were analysed from the diamicton units (Fig. 9). This comprised 252 clasts from Facies Group I and 240 clasts from Facies Group II. The average plunge for the clasts axes was 43° for Faces Group I and 42° for Facies Group II. Eigen values for Facies Group I were $S_1 = 0.46$, $S_2 = 0.31$ and $S_3 = 0.22$. Eigen values for Facies Group II were $S_1 = 0.45$, $S_2 = 0.32$ and $S_3 = 0.23$. Tests for a non-random distribution of clast azimuths (Rayleigh's R, Rao's U and Chi^2) all indicated no preferred orientation as they were above the threshold of $p < 0.05$. P values for Rayleigh's R, Rao's U and Chi^2 for Facies Group I were 0.11, 0.45 and 0.69. P values for Rayleigh's R, Rao's U and Chi^2 for Facies Group II were 0.37, 0.37 and 0.22.

4.7. Estimating local ground shaking due to past earthquakes

Results from the analysis of historic earthquake record are presented in Fig. 10. Only earthquakes that can produce MMI ≥6 are shown as there is a very low probability of landslides or rockfalls below this value (Robinson et al., 2016). The Amuri Earthquake of 1888 AD ($M_W = 7.4$) could produce the most intense ground shaking in the Chappa'ai catchment, with a maximum MMI of 9. The Amuri Earthquake occurred in late August at a time when Lake Chappa'ai most likely had ice cover. There were three earthquakes capable of producing a maximum MMI of 8. Two of these earthquakes occurred in 1929 and were north of Chappa'ai, while the other was SW of the study site (Fig. 10). The 1929 AD Murchison earthquake (north of Chappa'ai, $M_W = 7.3$) occurred during the period of ice cover on the lake (June). The other un-named earthquake in 1929 SW of Chappa'ai ($M_W = 7.01$) would have occurred in the ice free season (March). The final earthquake that could produce a maximum MMI of 8 was the 1968 AD Inangahua earthquake ($M_W = 7.1$). This earthquake occurred on the 23rd of May which is close to the end of the ice free season.

MMI isoseismals for prehistoric earthquakes are depicted in Fig. 11. All recorded prehistoric earthquakes on the central section of the Hope Fault could produce a maximum MMI of 9. Of the five Alpine Fault earthquakes, only the 1594 A.D. event could produce a maximum MMI of 9. The maximum proposed extent of other nearby Alpine Fault earthquakes (Howarth et al., 2014, 2016) would produce a maximum MMI of 8 (1717 A.D.) or 7 (1389–1409 AD, 1055–1107 A.D. and 894–961 A.D.). The rupture extent of the 290–530 A.D. Clarence Fault earthquake is not known, but an earthquake centred on the study site of Knuepfer (1992) could produce a maximum MMI of 9.

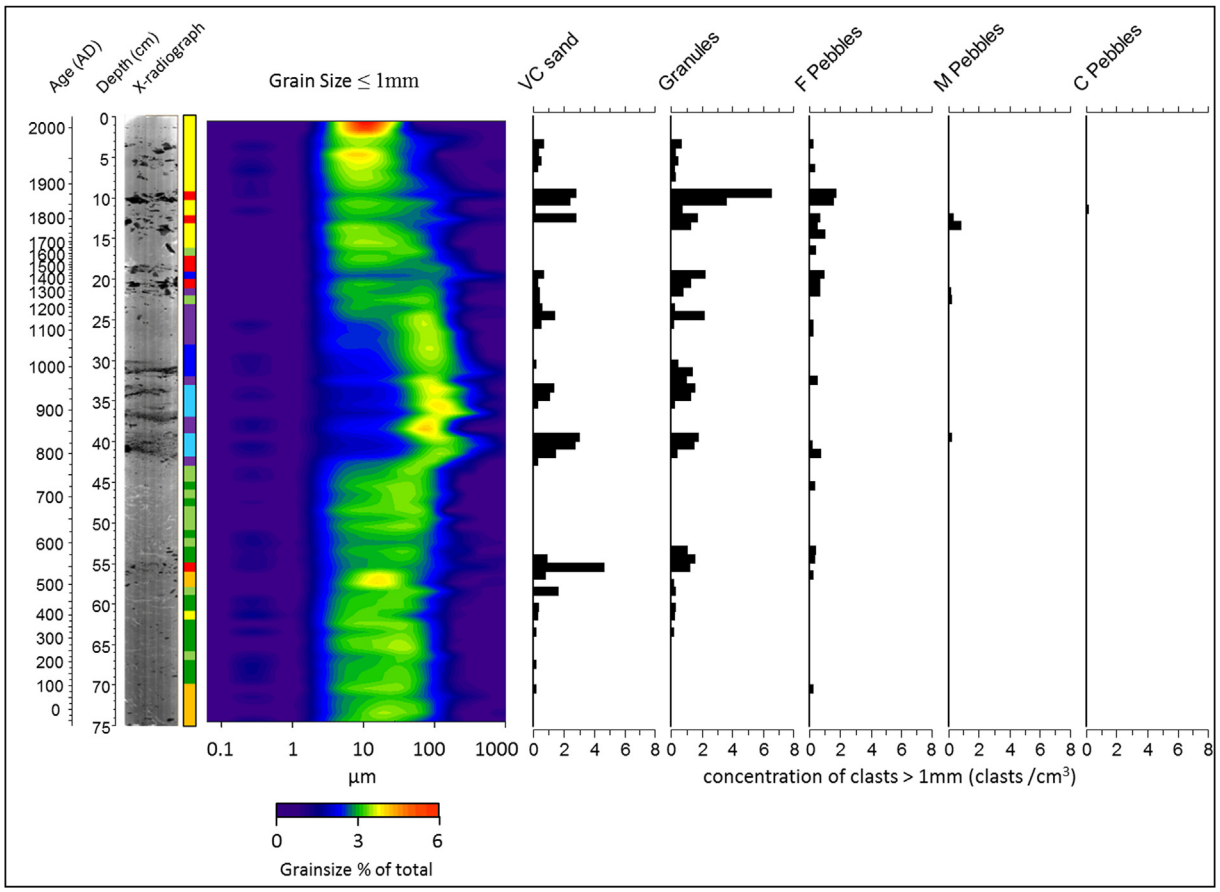

Fig. 6. Contour plot of ≤1 mm grain size analysis results and concentration of large (> 1 mm) clasts in CHLC. The X-radiograph and concentration of >1 mm clasts indicates the position of five main diamicton horizons. The contour plot clearly shows the increase in mean and modal grain size between ca. 23 and 40 cm.

5. Discussion

5.1. Chronology

No obvious macrofossils were identified during core sectioning and sub-sampling. The radiocarbon chronology relies on bulk sediment dates that are affected by an old carbon effect. The paired $^{14}C/^{210}Pb$ dates from the top part of CHLC are offset by ca. 840 years. Howarth et al. (2013) identified sources of old carbon in a study of bulk sediment radiocarbon ages from a New Zealand lake that are applicable here. Pollen, particulate organic carbon (POC) and bulk humic dates were up to 1400 years older than dates on leaf fossils from terrestrial plants. POC and dissolved organic carbon can be sourced from erosion of catchment soils and bedrock. Hilton et al. (2008) also demonstrated that an average of 37% of the POC discharged from mountain catchments in the Southern Alps is sourced from bedrock-derived fossil organic carbon. The current age model therefore provides an estimate of the age of deposition of the diamicton units beyond the range of ^{210}Pb. We should be aware that the contribution of old carbon could change through time (Zhou et al., 2015). Changes in lithofacies could be indicative of changes in lake and catchment processes and these could affect the delivery of old carbon to the lake sediments.

5.2. Transport mechanism for the large clasts

The large clasts in Facies Group I meet the criteria of dropstones as defined by Bennett et al. (1996). The presence of pebble sized clasts (Fig. 6) in a silty matrix (Fig. 7) represents a hydrodynamic paradox. There is a contrast between low energy depositional processes required to transport the host sediment, and the large clasts. Deposition of large clasts in this setting requires a rafting agent, and lake ice is the most obvious agent in this lake. There is not such a clear contrast between the size of the large clasts in Facies Group II and the matrix (Figs. 6 and 7). However, the clast fabric statistics (Fig. 9) also suggest that these are ice rafted debris.

Clast fabric in the diamicton units from both facies groups meet the criteria identified by Domack and Lawson (1985) for ice rafted debris. Clast azimuths showed no preferred orientation and clast plunges axes were steep (mean = 42–43°). Two eigen value ratios are key to eliminating a glacigenic origin for the Lake Chappa'ai diamicton deposits (Fig. 9). These ratios are $S_3{:}S_1$ (a measure of isotropy) and 1 - ($S_2{:}S_1$) which separates cluster (high values) from girdle fabrics (low values). Bennett et al. (1999) provide a review of clast fabrics for glacial diamicts. The poor clustering of the Lake Chappa'ai diamicton clast fabrics (1 - ($S_2{:}S_1$) = 0.29–0.33) excludes till deposits. Glacigenic flow deposits are also poorly clustered, but the Lake Chappa'ai diamicts are much more isotropic ($S_3{:}S_1$ = 0.47–0.51) than glacigenic flow deposits ($S_3{:}S_1$ < 0.4).

The available data strongly supports that the clasts were transported to the centre of the lake by ice rafting, but we still need to explain which process or processes produced the clasts. In the introduction we proposed that there are two main categories of hypotheses for diamicton formation; those that involve significant regional events or change, and those that invoke stochastic lake and catchment processes. We first examine if the diamicton deposits

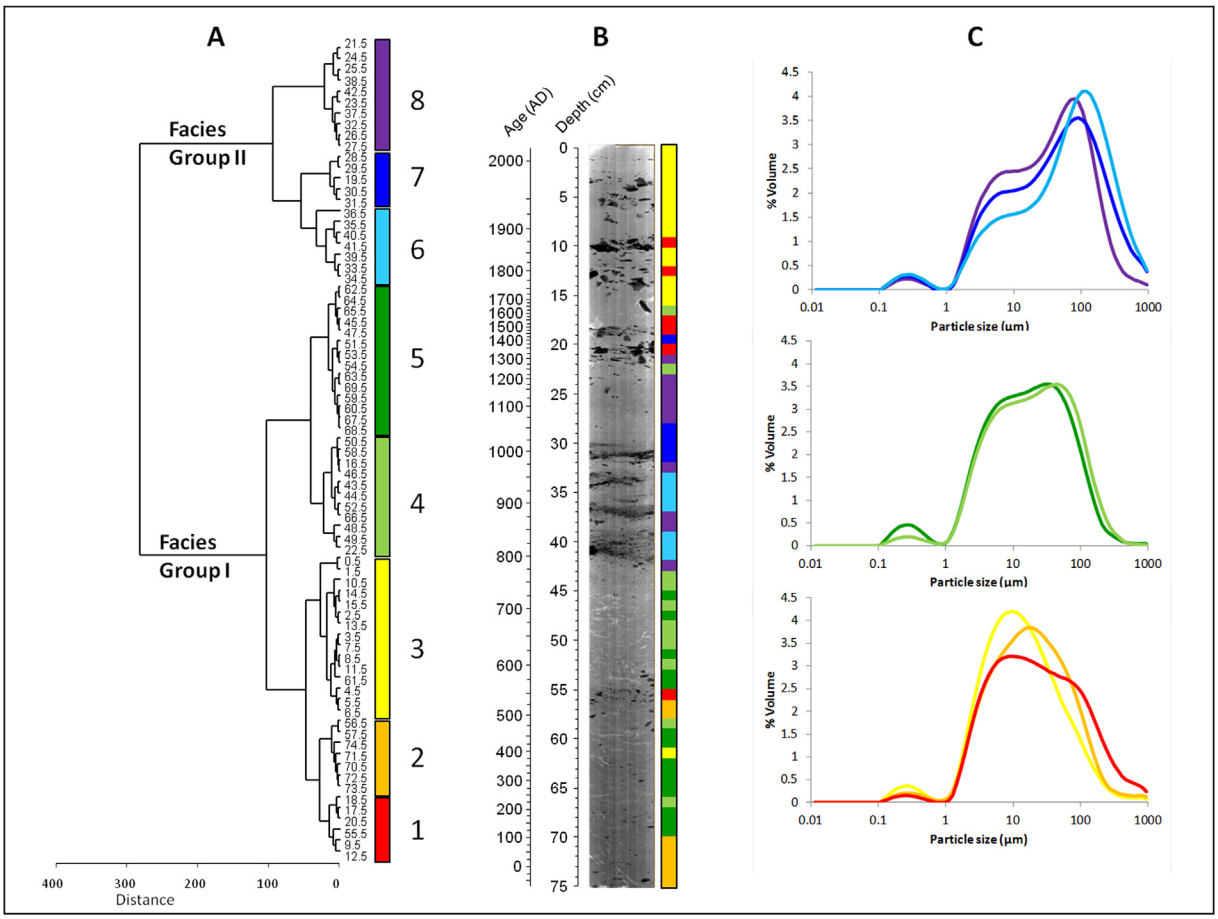

Fig. 7. Cluster analysis results for lithofacies analysis and ≤1 mm grain size distributions for each of the eight lithofacies. A. Cluster analysis was performed on 30 Itrax XRF and grain size variables. The eight lithofacies are separated into two main facies groups, Facies Group I and Facies Group II. B. X-radiograph of CHLC alongside the results for the lithofacies cluster analysis in A. C. Grain size distributions for the ≤1 mm fraction for each of the eight facies. The main differences between Facies Group I and II are the abundance of sand, skewness, mean and modal grainsize.

could represent random dumps of ice rafted debris onto the core sites by comparing the stratigraphy from CHLC and CHGC.

5.3. Comparison of >1 mm clast stratigraphies from both cores

A comparison of clast stratigraphies between CHLC and CHGC is provided in Fig. 4. From this data we conclude that most diamicton deposits are widespread in the lake basin and are likely to represent significant events. We could also conclude that some diamicts represent variability in deposition of dropstones following events, or background variability due to stochastic processes. However, we argue that the clast flux data may give a false impression of the degree of intra-lake variability. We examine some issues with the clast flux data that can easily be resolved in future studies. In short, gravity core extrusion and sub-sampling bias in both cores may result in the loss of some clast flux peaks.

First, we are comparing cores that were sampled using different techniques. Micro CT images (Fig. 9) indicate that coring can push down large clasts, especially those near the core barrel. Clasts will also be moved during extrusion of a gravity core and this may result in the loss of some clast peaks. We can avoid sampling the edge of the core while sub-sampling CHLC, but we cannot do this with the extruded gravity core samples from CHGC. Sub-sampling effects for both cores should also be considered. We took large (3 ml) samples for grainsize analysis, but in some cases variation in clast density visible in the Itrax X-rays, is not reflected in the clast counts. This appears to occur in CHLC between 18 and 22 cm. There are two clusters of clasts which are quite clear in the Itrax X-ray and micro-CT imagery (Figs. 4 and 9), but these clusters are not resolved in the clast flux stratigraphy (Fig. 4). We should also consider the effect of sub-sampling on the recorded stratigraphic position of large clasts since they could span multiple sample intervals. This should have a minor effect on the total clasts counts as most of the large clasts are smaller than 4 mm (granules and smaller, Fig. 6). This is smaller than the sample interval for the percussion and gravity cores. An easy solution to the sub-sampling bias issue is to count clasts with the micro-CT scanner. This would also allow identification and digital exclusion of clasts obviously displaced by coring.

If there is actually some intra-lake variability in clast deposition, a composite clast stratigraphy could be constructed for this lake. This approach was taken by Tomkins et al. (2009) who examined changes in ice cover using ice-rafted sedimentary pellets in a Canadian lake. We believe at this stage the lithofacies framework is the most reliable indicator of changes in stratigraphy in CHLC. This does include data from >1 mm clast stratigraphies, but there are 25 other variables used to construct the lithofacies classification.

5.4. Environmental significance of the diamicton layers

We propose in the following sections that Facies 1 diamicts can be attributed to large (MMI > 8) earthquake events on nearby faults. Facies 1 diamicts probably require the earthquake to occur in

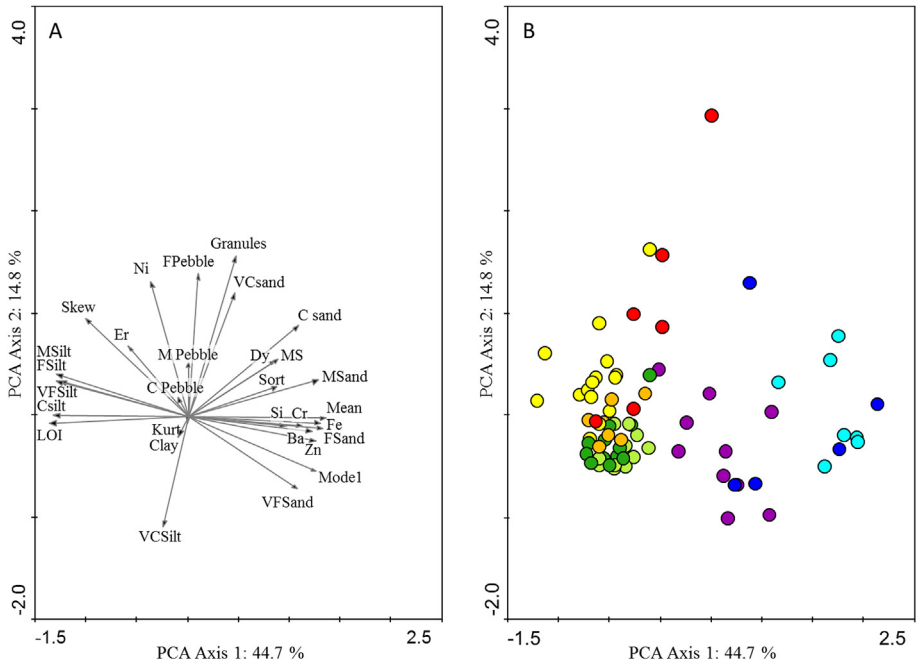

Fig. 8. PCA plot of samples from CHLC constrained by the 30 variables used in the lithofacies analysis. Sample positions are colour coded by the results of the cluster analysis depicted in Fig. 7. PCA axis 1 represents a mean and modal grainsize gradient for the ≤1 mm fraction and change in organic content (LOI). PCA axis 2 represents changes in the abundance of large (>1 mm) clasts. Er, Ni, Si, Cr, Fe, Ba, Zn are elemental symbols from Itrax XRF analysis. Abbreviations for other variables are: LOI = loss on ignition (organic content), MS = magnetic susceptibility. Prefixes for each size fraction (silt, sand, granules and pebbles) are F = fine, M = medium, C = coarse and VC = very coarse. Abbreviations for ≤ 1 mm grainsize properties are: Skew = skewness, Mean = mean grainsize, Mode1 = grainsize of Mode 1, Kurt = kurtosis. (For interpretation of the references to colour in this figure legend, the reader is referred to the web version of this article.)

winter so the rockfall generated by the earthquake is transported directly onto lake ice. Other Facies Group I diamicts could be attributed to either MMI >8 earthquakes occurring during the ice-free season, MMI ≤8 earthquakes occurring in winter, or other processes (e.g. climate change). Facies Group II diamicts do not have any analogues in the historical record so we can only speculate if these were caused by earthquakes, other catchment or climate related processes, or a combination of all of these processes.

5.4.1. *Facies 1 deposits as indicators of MMI >8 earthquakes*

The Facies 1 diamicts could represent rockfalls triggered by either large earthquakes on the faults in the vicinity of Lake Chappa'ai (Fig. 1) or stochastic collapse of the rock face to the west of the lake. There is some steep terrain to the west of the lake with rock outcrops that could provide a source of large clasts (Fig. 2). There are also large boulders near the shore on the western side of the lake (Supplementary Fig. 5, Appendix A) and these could have been produced by rockfalls. Either event could transport large clasts onto the top of lake ice during the winter. If such events occurred during the ice free season, subsequent instability of the catchment could still result in rockfalls onto lake ice in the following winter or winters.

The sedimentology of Facies 1 is inconsistent with other processes that could transport large clasts onto lake ice. Snow avalanches can transport large clasts onto lake ice, but the grainsize distribution of snow avalanche deposits is strongly polymodal (Vasskog et al., 2011), and snow avalanches incorporate macroscopic plant remains (Nesje et al., 2007; Korup and Rixen, 2014). These features are absent in Facies 1. The <1 mm sediment was bimodal (Fig. 7) and we did not observe any macroscopic remains from terrestrial plants. The coincidence of spring rainfall with the timing of snow melt leads to rain-on-snow events (Sánchez-López et al., 2016). Rain-on-snow events can lead to intense runoff episodes which can also transport large clasts to an ice covered lake (Sánchez-López et al., 2016). However, the grainsize distribution is not what would be expected for a high energy flood deposit, since there is a low (<25%) abundance of sand in the <1 mm fraction. Flood deposits capable of transporting large clasts should also contain abundant (>25%) sand (Lenzi and Marchi, 2000). There is not always an increase in sand content in Facies 1 deposits compared to underlying sediments (Fig. 5) and the grainsize of mode 1 is the second lowest value out of all of the facies units.

There were no obvious sedimentary structures typical of earthquake shaking (Rodríguez-Pascua et al., 2000). Attribution of diamicton deposits to earthquakes requires that coeval diamicts are visible in multiple lake catchments or synchronous with the timing of earthquakes dated from other records. The age of the Facies 1 unit between 9 and 10 cm in CHLC is 1852–1902 A.D. and this overlaps with the timing of the M_W 7.1, 1888 A.D. Amuri Earthquake (Fig. 12). Observations of earthquake damage (Cowan, 1989) indicate that the Lake Chappa'ai catchment was in the zone of MMI > 8, which is in agreement with our MMI estimates of MMI 8–9 (Fig. 11). The 1888 A.D. Amuri Earthquake was the only earthquake in the historic record that corresponded to the age of a Facies 1 deposit, and it was the only earthquake to produce MMI >8 shaking in the Chappa'ai catchment (Fig. 10). This provides strong evidence for a lower MMI threshold of 8 for producing Facies 1 units. Facies 1 units contain the highest concentration of large clasts (Table 2, Appendix A) and MMI > 8 shaking is probably necessary to produce a large amount of clasts > 1 mm.

We should also consider the effect of changing lake ice cover as it is possible that a MMI >8 earthquake that occurs in the ice free season might not result in the production of a Facies 1 deposit. The Amuri Earthquake occurred in August, a time when there would have been ice cover on the lake. We do not have enough data to determine if a MMI >8 earthquake occurring in the ice free season

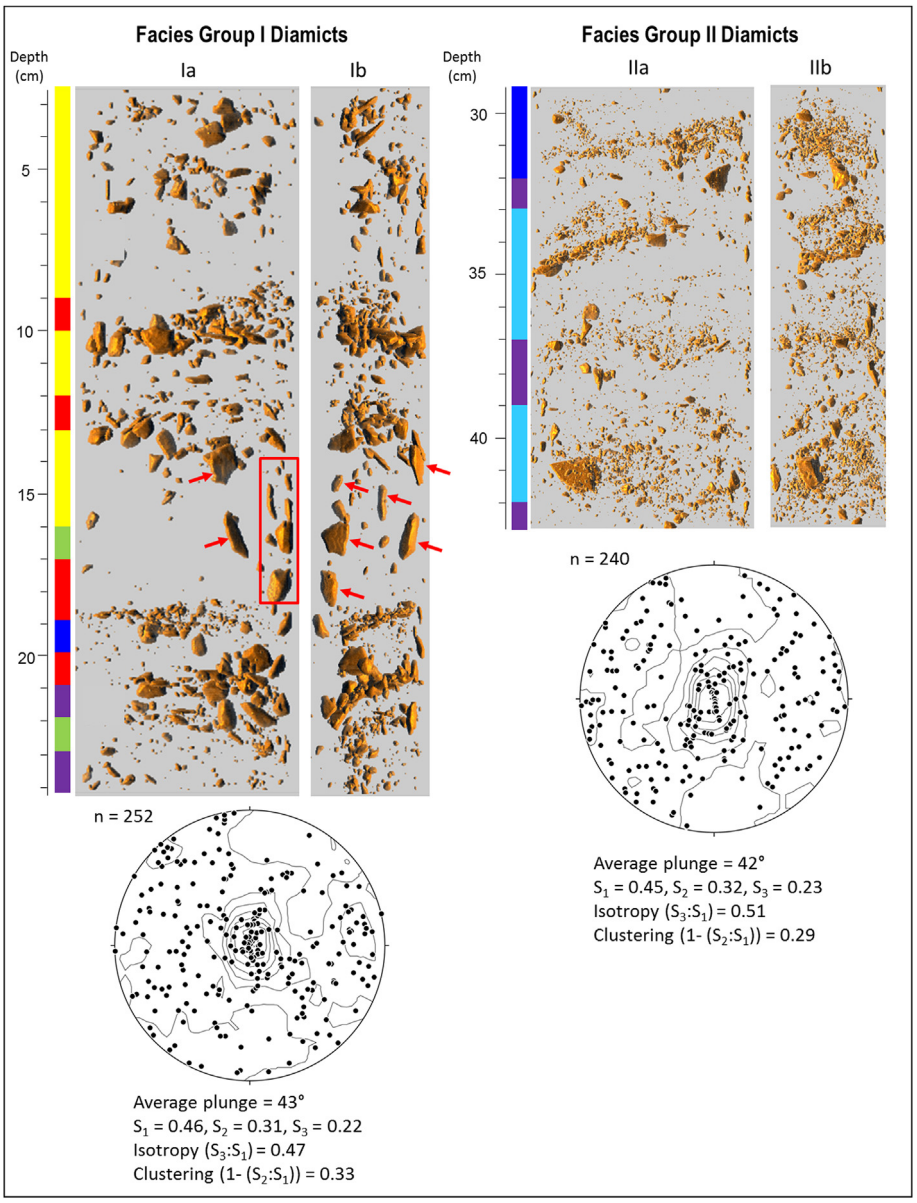

Fig. 9. Micro Computed Tomography (CT) scan results for Facies Group I and II from CHLC. Images show views perpendicular to the sectioned core surface (Ia and IIa) and lateral views (Ib and IIb). Red arrows and the red box show the position of clasts most likely pushed down into lower sediments during coring. Stereoplots show the azimuth and plunge of all clasts with long axes > 1 mm with a:b axial ratios >1.5. Average plunges, eigen values (S_1, S_2, S_3), and measures of isotropy and clustering are provided for each facies group. The coloured sections to the left of the CT images indicate facies units using the key from Fig. 7. (For interpretation of the references to colour in this figure legend, the reader is referred to the web version of this article.)

would still produce a Facies 1 deposit. There is only one earthquake capable of producing MMI >8 in the historical record. We propose as a testable hypothesis that the Facies 1 deposits represent primary earthquake triggered rockfall deposits. Facies 1 units might only be produced if an earthquake occurs in winter and the rockfall travels directly onto lake ice. MMI >8 earthquakes in the ice free season may still be represented as an increase in large clasts if they cause instability in the catchment and subsequent rockfalls in winter. We compared the Chappa'ai diamict record with earthquake records from other sources (Knuepfer, 1992; Howarth et al., 2014, 2016; Khajavi et al., 2016) to explore this possibility.

There were eight earthquakes over the last 2000 years that would have produced MMI >8 in the Chappa'ai catchment and there were only five Facies 1 units (Figs. 11 and 12). The 1888, 1740–1840, 1479–1623 A.D. Hope Fault earthquakes (Khajavi et al., 2016) have corresponding Facies 1 units. The 1545–1594 A.D. Alpine Fault earthquake (Howarth et al., 2014) also overlaps the time range of one of the Facies 1 units. The lowest Facies 1 unit could correspond to either the 373–419 or 439–551 A.D. Hope Fault earthquakes (Khajavi et al., 2016) or the 290–530 A.D. Clarence Fault earthquake (Knuepfer, 1992). Only the 819–1092 A.D. Hope Fault earthquake could possibly be attributed to a non-Facies 1 diamict (see discussion below on other facies units) so this leaves two MMI > 8 earthquakes between 300 and 550 A.D. not represented by Facies 1 units.

There are several possible explanations for the missing of a Facies 1 unit between 300 and 550 A.D. MMI predictions for Hope Fault earthquakes are based on maximum possible earthquake magnitudes for this fault. It is possible that two of these earthquakes were too small to produce MMI >8 at Lake Chappa'ai. The

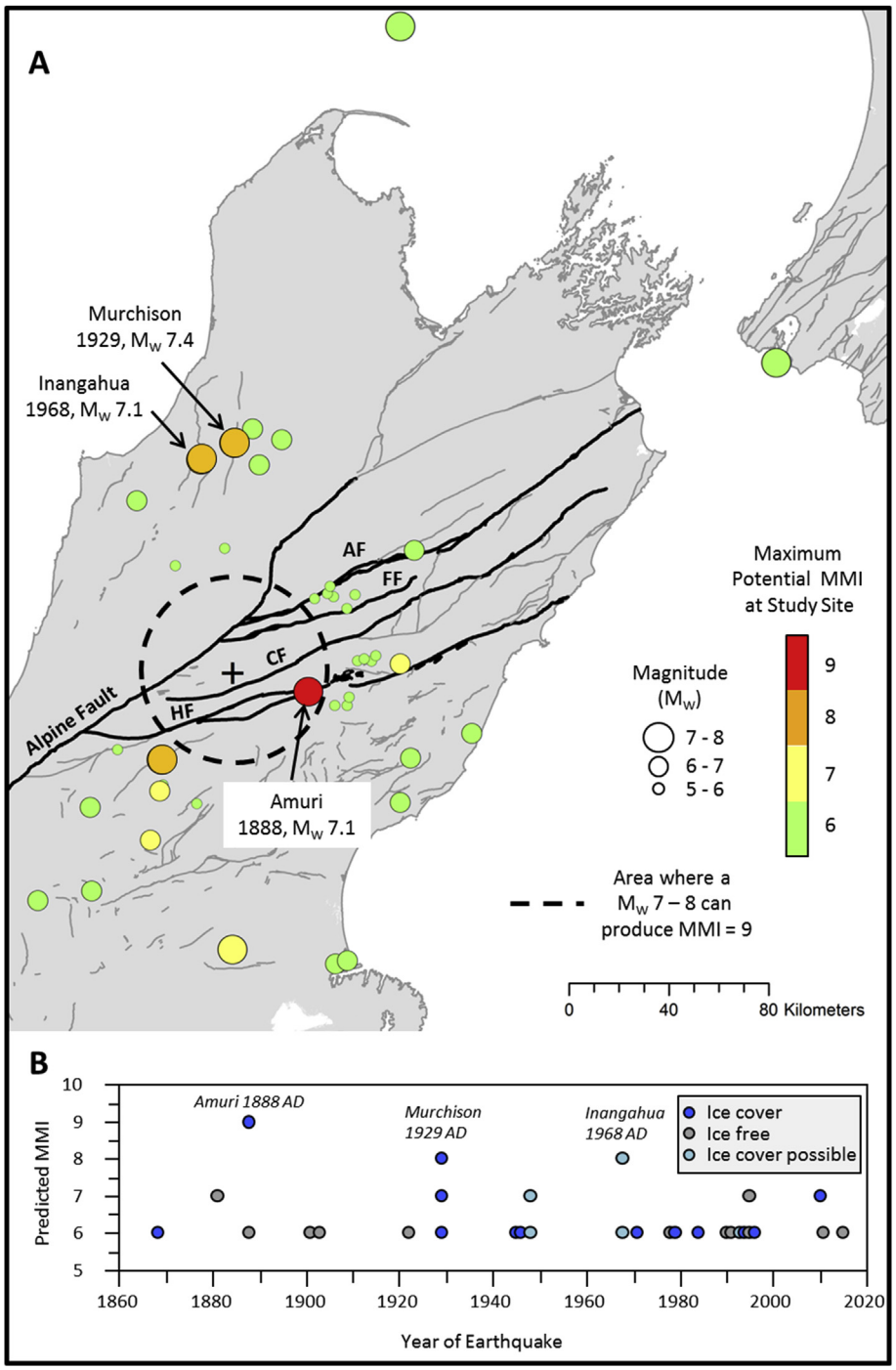

Fig. 10. Results of the sensitivity analysis for earthquake magnitude and seasonality. A. The location of earthquakes in the historical record capable of producing shaking equivalent to MMI ≥6 in the Chappa'ai catchment. The location of Chappa'ai is shown by a black cross. The dashed circle indicates the area where a M_W 7–8 earthquakes can produce MMI >8. Epicentres for three large earthquakes (Amuri, Inangahua and Murchison) discussed in the text are also shown. HF = Hope Fault, CF = Clarence Fault, FF = Fowler Fault, AF = Awatere Fault B. Predicted MMI in the Lake Chappa'ai catchment for historical earthquakes colour coded by the presence or absence of ice cover on Lake Chappa'ai at the time of the earthquake. (For interpretation of the references to colour in this figure legend, the reader is referred to the web version of this article.)

Hope Fault earthquake history presented in Fig. 12 represents one interpretation of the Hope Fault record reported by Khajavi et al. (2016). Critically, Khajavi et al. (2016) only observed evidence for two Hope Fault earthquakes between 300 and 550 A.D. in one of their two fault trench sites. The other fault trench site indicated only one earthquake during this period, and this was corroborated by other evidence in the surrounding landscape. This interpretation would still leave one event without a Facies 1 unit. The final possibility is that the two missing earthquakes occurred in the ice free season. The peaks in clast flux below Facies 1 between 300 and 550 A.D. could correspond to these earthquakes (Fig. 12) and represent subsequent catchment instability and rock falls when the lake had ice cover. We discuss this possibility in detail in the next section.

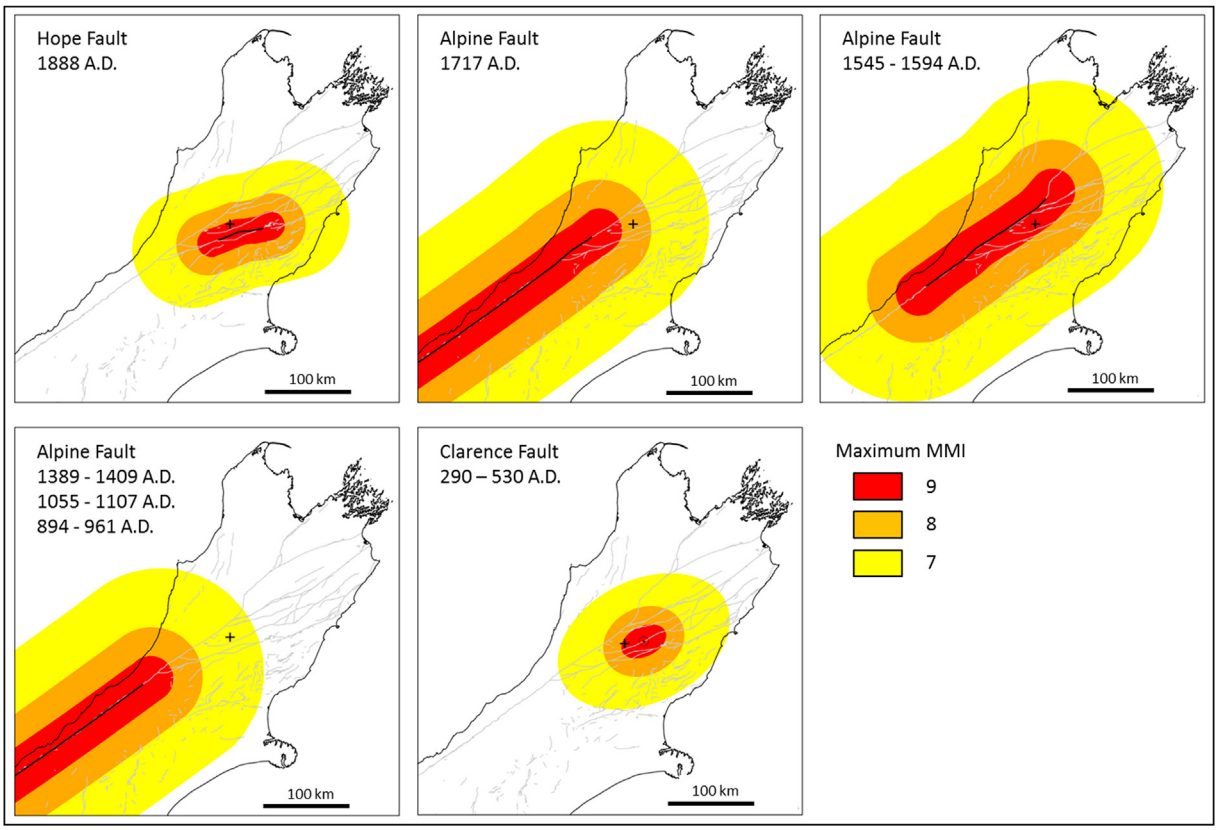

Fig. 11. Calculated maximum shaking in terms of Modified Mercalli Intensity (MMI) produced by earthquakes on major faults near Lake Chappa'ai. Isoseismals for major prehistoric earthquakes are based on the inferred rupture extents from Howarth et al. (2014, 2016) and Khajavi et al. (2016). There was no information on the extent of the 290–530 A.D. Clarence Fault rupture, so the isoseismals are centred on the study site of Knuepfer (1992). The location of Lake Chappa'ai is shown by a black cross.

5.4.2. Other Facies Group I diamicts

Other diamict deposits in Facies Group I could be caused by MMI 7–8 earthquakes when the lake has ice cover, MMI >8 earthquakes in the ice free season, stochastic lake and catchment processes, or a response of the lake and catchment to climate change.

Diamict deposits in Facies Group I that do not belong to Facies 1 are most common in the upper 10 cm and lower 20 cm of CHLC (Fig. 6). These could be caused by MMI 7–8 earthquakes that occurred when the lake had ice cover. The uppermost Facies Group I diamicts were deposited after 1900 A.D. (Fig. 12). It is possible for the upper diamicts to represent MMI 7–8 earthquakes. At least one of the diamict units in the upper 10 cm of CHLC was also present in CHGC (Fig. 4). The overlap of the 95% confidence intervals from the age models from CHLC and CHGC is 1964–1970 A.D (Fig. 4). This time-period overlaps with a significant earthquake (M_W 7.1) on the Inangahua-Maimai Fault (Fig. 10) that occurred in 1968 A.D. (Barnes and Ghisetti, 2016). We estimated a maximum MMI of 8 for this earthquake at Lake Chappa'ai (Fig. 10), which is in agreement with estimates based on damage from this earthquake (Berrill et al., 1988). The Inangahua-Maimai earthquake occurred on the 23rd of May 1968 which is at a time when it is possible that Lake Chappa'ai had ice cover. There is also a peak in clast flux in CHLC that occurs between 1925 and 1950 A.D. (Fig. 4). This corresponds to the 1929 A.D. M_W 7.6 Murchison Earthquake (Fig. 10). Observations of earthquake damage indicate that this earthquake would have produced MMI 8 which matches with our estimates of MMI $\leq$8 (Fig. 10).

Two of the Facies Group I diamicts below the lowest Facies 1 diamict (Fig. 12) could be attributed to either the Hope or Alpine MMI >8 earthquakes from between 300 and 500 A.D. (Fig. 12). If these earthquakes occurred in the ice free season, any rockfalls triggered during the earthquake would not have fallen directly onto the lake ice. We need to be cautious about this interpretation as we cannot rule out intra-lake stochastic processes (we don't have a matching core for this time period) or other regional changes such as climate. We rule out floods and snow avalanches as a cause for the lower diamicts. They lack a significant concentration of sand (Lenzi and Marchi, 2000), the <1 mm grainsize distribution is not polymodal (Vasskog et al., 2011) and there is an absence of plant macrofossils (Nesje et al., 2007; Korup and Rixen, 2014).

There are limited climate records spanning the last 2000 years in New Zealand. Lorrey et al. (2008) examined climate proxies from New Zealand spanning the last ca. 4000 years. These records came from the western South Island and eastern North Island (Fig. 12). The $\delta^{18}O$ record was interpreted by Lorrey et al. (2008) as a temperature proxy. Some of the coldest inferred temperatures for the last 2000 years occur between 0 and 500 A.D. and correspond to the presence of higher >1 mm fluxes. Colder temperatures could lead to increased frost shattering of rock in the catchment (Matsuoka, 2001) or a thicker ice cover (Leppäranta, 2015). Thickening of the ice cover may increase contact with littoral sediments and increase the flux of ice rafted debris. We should be cautious about making inferences based on the speleothem based climate reconstruction. As we will discuss in the following section, reconstructions based on the western South Island speleothem records conflict with other proxies, such as the tree ring record from Oroko Swamp (Fig. 12; Cook et al., 2002). There are also very large uncertainties on the age control of the speleothem record.

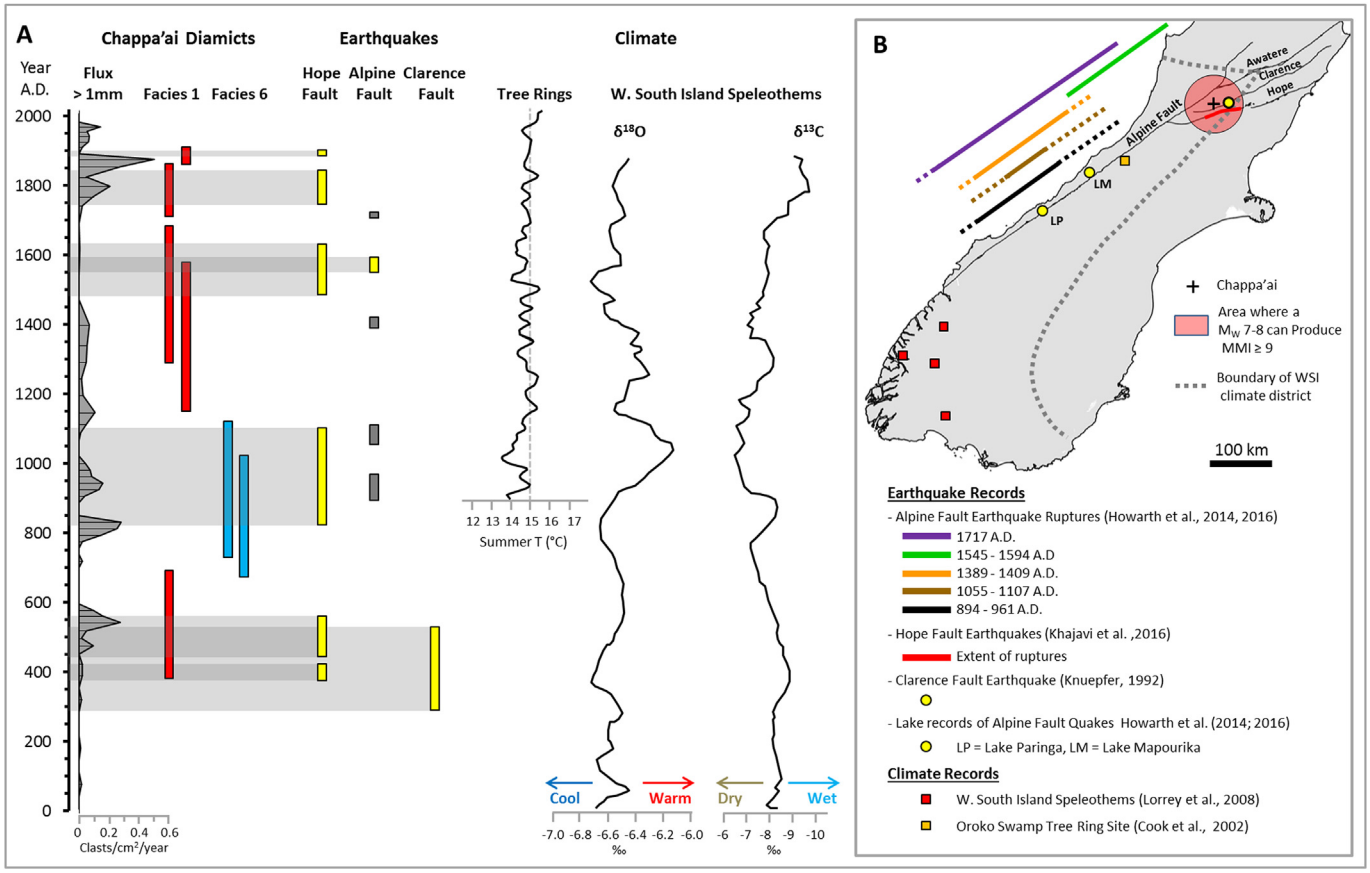

Fig. 12. Comparison of the Lake Chappa'ai diamicton record with relevant earthquake and climate records. A. Diamict clast flux and age of Facies 1 and 6 units compared to earthquake and climate records. Age uncertainties take into account the depth span of the facies unit (they are not simply mid-point ages) and are 95% confidence intervals. The ages of diamict units are compared with the timing of past earthquakes and paleoclimate records for the Western South Island climate district. Earthquakes capable of producing MMI >8 in the Lake Chapp'ai catchment are yellow, with other earthquakes shown in grey. B. The location of relevant earthquake records and the extent of the inferred rupture of pre-historic earthquakes. The location of western South Island speleothem records and tree ring record are also depicted. (For interpretation of the references to colour in this figure legend, the reader is referred to the web version of this article.)

5.4.3. *Facies group II diamicts*

The diamicton layers in Facies Group II are quite different to the deposits in Facies Group I. The matrix is much sandier (Figs. 5–8, Supplementary Table 2 Appendix A), and the >1 mm clasts are not grouped in tightly clustered horizons (Fig. 9). The X-radiograph and micro CT images (Figs. 7 and 9) reveal that the diamicton deposits in Facies Group II are also laterally discontinuous. The clasts in these diamicton units also tend to be smaller, with a low concentration of pebbles (Fig. 6). The highest concentration of clasts >1 mm in Facies Group II occurs in Facies 6 (Figs. 5 and 6). There are two Facies 6 units between 33 and 42 cm in CHLC (Fig. 7).

We do not have enough information to conclusively determine the process or processes causing the formation of Facies Group II diamicts. Some processes can be eliminated, but more data is required to provide a definitive answer. We only have estimates of ground shaking intensity required to produce Facies Group I diamicts. MMI >8 is required to produce Facies 1 diamicts, but it appears that MMI 7–8 might result in enough shaking in the catchment to produce an increase in >1 mm clast flux to the lake. There was one earthquake on the Hope Fault is capable of producing a MMI >8 earthquake between 819 and 1092 A.D. (Fig. 12). The timing of the Hope Fault earthquake overlaps with the age of both Facies 6 units and peaks in clast concentration (Fig. 12). This only accounts for one of the two Facies 6 units. The inferred extent of the 894–961 A.D. and 1055–1107 A.D. Alpine Fault earthquakes (Howarth et al., 2014, 2016, Fig. 12) means that they would result in shaking equivalent to MMI ≤7 in the Chapp'ai catchment (Fig. 11). The data we have from Facies Group I diamicts indicates that MMI >7 is required to trigger rockfalls in the lake catchment. If we accept an earthquake trigger for the Facies 6 diamicts (which we caution against at this stage) we would need to extend the inferred rupture of one of the Alpine Fault earthquakes to the north so that the Chappa'ai catchment lies within the zone of MMI > 7.

Changing climate and its effect on lake and catchment processes could also lead to Facies Group II diamict formation. Climate change can affect processes leading to snow avalanches onto lake ice (Nesje et al., 2007), flooding (Sánchez-López et al., 2016; Fouinat et al., 2017), or adfreezing of littoral lake deposits onto anchor ice (Kempema et al., 2001). Strong winds can also transport large clasts onto the surface of lake ice (Spaulding et al., 1997). In the following section we will discuss the state of Late Holocene New Zealand paleoclimate records and evidence for the effect of the aforementioned climate processes on diamict formation in Lake Chappa'ai.

The only climate records with sufficient resolution spanning the last 2000 years are the western South Island speleothem records (Lorrey et al., 2008) and the mean annual temperature (MAT) tree-ring based reconstruction from Oroko Swamp (Cook et al., 2002) (Fig. 12). There are two problems with using these climate records. First, the speleothems and tree-rings appear to produce conflicting reconstructions, with the speleothems inferring the warmest period for the last 2000 years around 1050 A.D. This warm period inferred from the speleothem records coincides with the coldest

inferred temperatures for the last 1100 years. Curiously, the interpretation of the western South Island speleothem record considered the Oroko Bog tree-ring record, so should have taken this into account. The other problem is the very large uncertainty on the age control of the speleothems. The speleothem chronology is based on a composite of five speleothems from the WSI. Only two of these speleothems have uranium series dates that span the last 2000 years. The two records only have a combined total of five age control points and some uranium series ages span up to 900 years (Lorrey et al., 2008).

Although we don't have consistent climate reconstructions from the western South Island, we can eliminate some climate related processes that may cause diamict formation. We can exclude wind as a transport mechanism for clasts >1 mm. Aeolian transport of clasts >1 mm does not appear to be tenable without a major change in catchment vegetation and/or massive increase in wind speed. There are limited observations of wind speeds in the New Zealand mountains, but available records indicate that wind speeds can frequently exceed 160 km/h, with maximum wind gusts reaching 240 km/h (McCracken, 1980). This is sufficient for Aeolian transport of sand by incipient suspension, but larger clasts can only be transported by saltation. Wind speeds in excess of 290 km/h are required to initiate incipient suspension of pebbles. Complete suspension of the >1 mm fraction requires wind speeds greater than 490 km/h (Eastwood et al., 2012). Catchment vegetation would prevent transport by saltation over long distances in this catchment (Zarnetske et al., 2012). Since the strongest winds originate from the NW, clasts would need to be transported from the scree over the ridge to the NW of Chappa'ai (Fig. 2). The lake catchment is vegetated right up to the edge of the lake (Supplementary Fig. 6) so currently there is not a beach that can supply < 1 mm clasts to the lake ice in winter. There is abundant sand and gravel in the littoral zone of the lake and this could only become a source of clasts if there was a drop in lake water level. We can also eliminate snow avalanche deposits as the <1 mm grain-size distributions are not polymodal (Vasskog et al., 2011) and there was an absence of terrestrial macrofossils (Nesje et al., 2007; Korup and Rixen, 2014).

This leaves two main possibilities for the Facies Group II diamicts; an increase in ice-rafted debris due to a change in ice cover (Kempema et al., 2001) or rain on snow events (Sánchez-López et al., 2016). The discontinuous nature of the Group II diamict layers superficially resembles iceberg dumps (Domack and Lawson, 1985) and the mixture of coarse and fine clasts (including sand) could represent adhesion of littoral sediments to the base of anchor ice. An increase in ice thickness could lead to increased contact of the base of the ice with littoral sediments. The littoral sediments in Chappa'ai contain coarse clasts >1 mm. Increased ice thickness can result from cooler temperatures and/or changes in snowfall. After ice cover formation, ice thickness continues to increase while the released latent heat from freezing and the heat flux from the lake water can be conducted through the ice to the atmosphere (Leppäranta, 2015). Early snowfalls can decelerate ice growth due to the low heat conductivity of snow (Leppäranta, 2015).

The coincidence of spring rainfall with the timing of snow melt leads to rain-on-snow events (Sánchez-López et al., 2016). Rain-on-snow events can lead to intense runoff episodes which can also transport large clasts to an ice covered lake (Sánchez-López et al., 2016). Rain-on-snow events require warmer spring temperatures caused by an earlier increase in temperature. This results in the coincidence of snowmelt with spring rainfalls (Sánchez-López et al., 2016). Since the Group II diamicts are ice rafted, this would also require the persistence of ice cover in warmer spring conditions. This would be possible if winter conditions were colder and/or if there an insulating layer of snow on the ice (Sánchez-López et al., 2016). Examination of the biological proxy record from Lake Chappa'ai, especially chironomids and diatoms would help to test these theories. Both proxies might give an indication of changes in ice cover and an increase in the abundance of littoral diatoms in the diamicts might indicate transport of littoral sediments to the lake centre (Smith, 2000). A chironomid-based temperature reconstruction using established New Zealand transfer functions (Woodward and Shulmeister, 2006; Dieffenbacher-Krall et al., 2007) from this site would also help to constrain the Late Holocene climate history for this time period.

6. Conclusions and future directions

The main aim of this study was to determine the processes that led to the formation of diamictic sediments in a New Zealand alpine lake. We used multiple techniques to create a facies classification for lake sediment diamicts and then considered hypotheses for the formation of different facies units. We are confident that Facies 1 diamicts represent earthquake triggered rockfalls onto lake ice. Comparison of the dates of diamict deposition with the historic earthquake record indicates that MMI >8 shaking in the lake catchment may be required to produce Facies 1 diamict units. It may also be necessary for an earthquake to occur when the lake has ice cover. Large earthquakes that occur when the lake does not have ice cover could result in catchment instability and rockfalls when the lake has ice cover, but these still might not produce a Facies 1 unit. Earthquakes that produce MMI 7–8 in the catchment or MMI >8 during the ice free season may result in an increase in large (>1 mm) clasts to the lake, but we should be careful to eliminate other processes that could lead to diamict formation (e.g. climate). We compared the diamict record from Lake Chappa'ai with the prehistoric earthquake record and it is possible that some MMI >8 earthquakes are not represented by Facies 1 units. This would lend support to the hypothesis that MMI >8 earthquakes need to occur when the lake has ice cover to produce Facies 1 units.

More work is required to establish the role of climate related processes on the formation of non-Facies 1 diamicts in Lake Chappa'ai. We did not have any historical analogues for some diamict facies and these could result from earthquakes or climate related processes. Facies Group II diamicts were deposited during a time when major changes are inferred from the paleoclimate record. However, inferences from different climate proxies (speleothems and tree-rings) appear to be conflicting and age control on speleothem records has large uncertainties. We were able to eliminate some climate related processes (wind, rain on snow events and snow avalanches) because of the diamict sedimentology. Transport of clasts by anchor ice or rain on snow events remained as a distinct possibility for the formation of Facies Group II diamicts. Additional data, such as a diatom or chironomid record from Lake Chappa'ai may help to resolve the contribution of climate processes to diamict formation. We also recommend the collection of more data on the mountain climate in New Zealand and the phenology of ice cover on New Zealand mountain lakes.

In summary, we have demonstrated that lakes with seasonal ice cover in seismically active settings will record the frequency of large (MMI > 8) earthquakes by the deposition of diamicton horizons. Currently, we should consider these records as an indicator of minimum earthquake activity until we can disentangle the effects of climate change on diamict formation. Changes in climate will affect how mountain lakes record earthquake events by altering the transport of large clasts to the centre of the lake by changing lake ice cover. At extreme ends of the spectrum, lakes that are ice free will not produce earthquake diamicts and lakes that have perennial

ice cover may produce a diamict representing multiple earthquakes if ice cover does eventually melt. A reduction in the duration of winter ice cover will also decrease the probability of capturing primary rockfall deposits from earthquakes. This study highlights the multiple mechanisms that can lead to diamict formation in mountain lake sediments. These processes should always be considered before attributing the presence of diamict deposits to ice-rafted debris in a pro-glacial lake. This is particularly true in seismically active settings where earthquake triggered rockfalls may lead to diamict formation.

Acknowledgments

We thank the New Zealand Department of Conservation for permission to sample Lake Chappa'ai. Many ANSTO scientists and technicians provided useful discussions, advice, and technical support for this project including Brodie Cutmore, Daniella Fierro, Henk Heijnis, Quan Hua, Krystyna Saunders and Alan Williams. We thank the anonymous reviewers for their feedback and suggestions on this manuscript. Funding for this project was provided by operating costs linked to a combined ANSTO/University of Queensland Postdoctoral Research Fellowship to CW and analyses provided by ANSTO scientists, technicians and infrastructure.

Appendix A. Supplementary data

Supplementary data related to this article can be found at https://doi.org/10.1016/j.quaint.2017.10.051.

References

Adams, J., 1980. Contemporary uplift and erosion of the southern Alps, New Zealand. Geol. Soc. Am. Bull. 91, 1–114.
Adrian, R., O'Reilly, C.M., Zagarese, H., Baines, S.B., Hessen, D.O., Keller, W., Livingstone, D.M., Sommaruga, R., Straile, D., Van Donk, E., Weyhenmeyer, G.A., Winderl, M., 2009. Lakes as sentinels of climate change. Limnol. Oceanogr. 54 (6), 2283–2297.
Agin, M.A., Godbole, A.P., 1992. A new exact runs test for randomness. In: LePage, R. (Ed.), Computing Science and Statistics. Springer, New York.
Allmendinger, R.W., Cardozo, N., Fisher, D., 2012. Structural Geology Algorithms: Vectors and Tensors in Structural Geology, vol. 2012. Cambridge University Press, p. 304.
Appleby, P.G., 2001. Chronostratigraphic techniques in recent sediments. In: Last, W.M., Smol, J.P. (Eds.), Tracking Environmental Change Using Lake Sediments. Volume I: Basin Analysis, Coring, and Chronological TechniquesKluwer Academic Publishers, Dordrecht, The Netherlands.
Bao, R., Hernandez, A., Saez, A., Giralt, S., Prego, R., Pueyo, J.J., Moreno, A., Valero-Garces, B.L., 2015. Climatic and lacustrine morphometric controls of diatom paleoproductivity in a tropical Andean lake. Quat. Sci. Rev. 129, 96–110.
Barnes, P.M., Ghisetti, F.C., 2016. Structure, late Quaternary slip rate and earthquake potential of marine reverse faults along the North Westland deformation front, New Zealand. N. Z. J. Geol. Geophys. 59 (1), 157–175.
Battarbee, R.W., Thompson, R., Catalan, J., Grytnes, J.A., Birks, H.J.B., 2002. Climate variability and ecosystem dynamics of remote alpine and arctic lakes: the MOLAR project. J. Paleolimnol. 28 (1), 1–6.
Bennett, M.R., Doyle, P., Mather, A.E., 1996. Dropstones: their origin and significance. Palaeogeogr. Palaeoclimatol. Palaeoecol. 121, 331–339.
Bennett, M.R., Waller, R.I., Glasser, N.F., Hambrey, M.J., Huddart, D., 1999. Glacigenic clast fabrics: genetic fingerprint or wishful thinking? J. Quat. Sci. 14 (2), 125–135.
Berrill, J.B., Bienvenu, V.C., Callaghan, M.W., 1988. Liquefaction in the Buller region in the 1929 and 1968 earthquakes. Bull. N. Z. Natl. Soc. Earthq. Eng. 21, 174–189.
Bird, B.W., Abbott, M.B., Rodbell, D.T., Vuille, M., 2011. Holocene tropical South American hydroclimate revealed from a decadally resolved lake sediment $\delta^{18}O$ record. Earth Planet. Sci. Lett. 310, 192–202.
Blaauw, M., Christen, J.A., 2011. Flexible paleoclimate age-depth models using an autoregressive gamma process. Bayesian Anal. 6, 457–474.
Blaauw, M., van Geel, B., Kristen, I., Verschuren, D., 2011. High-resolution ^{14}C dating of a 25,000-year lake-sediment record from equatorial East Africa. Quat. Sci. Rev. 30 (21), 3043–3059.
Blott, S.J., Pye, K., 2001. GRADISTAT: a grain size distribution and statistics package for the analysis of unconsolidated sediments. Earth Surf. Process. Landforms 26 (11), 1237–1248.
Cardozo, N., Allmendinger, R.W., 2013. Spherical projections with OSXStereonet. Comput. Geosci. 51, 193–205.
Catalan, J., Pla, S., Rieradevall, M., Felip, M., Ventura, M., Buchaca, T., Camarero, L., Brancelj, A., Appleby, P.G., Lami, A., Grytnes, A., Agusti-Panareda, A., Thompson, R., 2002. Lake Redo ecosystem response to an increasing warming in the Pyrenees during the twentieth century. J. Paleolimnol. 28 (1), 129–145.
Clark, M., Hreinsson, E.Ö., Martinez, G., Tait, A., Slater, A., Hendrikx, J., Owens, I., Gupta, H., Schmidt, J., Woods, R., 2009. Simulations of seasonal snow for the South Island, New Zealand. J. Hydrol. 48 (2), 41–58.
Cowan, H.A., 1989. An Evaluation of the Late Quaternary Displacements and Seismic Hazard Associated with the Hope and Kakapo Faults, Amuri District, North Canterbury. M.Sc. thesis. University of Canterbury, New Zealand, p. 239.
Cook, E.R., Palmer, J.G., D'Arrigo, R.D., 2002. Evidence for a 'Medieval Warm Period' in a 1,100 year tree-ring reconstruction of past austral summer temperatures in New Zealand. Geophys. Res. Lett. 29 (14), 1667.
Cox, S.C., Stirling, M.W., Herman, F., Gerstenberger, M., Ristau, J., 2012. Potentially active faults in the rapidly eroding landscape adjacent to the Alpine fault, central Southern Alps, New Zealand. Tectonics 31, TC2011.
Davies, S.J., Lamb, H.F., Roberts, S.J., 2015. Micro-XRF core scanning in paleolimnology: recent developments. In: Croudace, I.W., Rothwell, R.G. (Eds.), Micro-XRF Studies of Sediment Cores, Developments in Paleoenvironmental Research. Springer Science and Business Media Dordrecht, p. 656.
De Jong, R., Schneider, T., Hernández–Almeida, I., Grosjean, M., 2016. Recent temperature trends in the South Central Andes reconstructed from sedimentary chrysophyte stomatocysts in Laguna Escondida (1742m a.s.l., 38°28S, Chile). Glob. Planet. Change 137, 24–34.
Dieffenbacher-Krall, A.C., Vandergoes, M.V., Denton, G.H., 2007. An inference model for mean summer air temperatures in the Southern Alps, New Zealand, using subfossil chironomids. Quat. Sci. Rev. 26, 2487–2504.
Domack, E.W., Lawson, D.E., 1985. Pebble fabric in an ice-rafted diamicton. J. Geol. 93 (5), 577–591.
Dowrick, D.J., Rhoades, D.A., 2005. Revised models for attenuation of modified mercalli intensity in New Zealand earthquakes. Bull. N. Z. Natl. Soc. Earthq. Eng. 38, 185–214.
Eastwood, E.N., Kocurek, G., Mohrig, D., Swanson, T., 2012. Methodology for reconstructing wind direction, wind speed and duration of wind events from aeolian cross-strata. J. Geophys. Res. 117, Fo3035.
Eyles, N., Eyles, C.H., Miall, A.D., 1983. Lithofacies types and vertical profile models; an alternative approach to the description and environmental interpretation of glacial diamict and diamictite sequences. Sedimentology 30, 393–410.
Fouinat, L., Sabatier, P., Poulenard, J., Reyss, J.-L., Montet, X., Arnaud, F., 2017. A new CT scan methodology to characterize a small aggregation gravel clast contained in a soft sediment matrix. Earth Surf. Dyn. 5, 199–209.
Glur, L., Wirth, S.B., Büntgen, U., Gilli, A., Haug, G.H., Schär, C., Beer, J., Anselmetti, F., 2013. Frequent floods in the European Alps coincide with cooler periods of the past 2500 years. Sci. Rep. 3. Article number 2770.
Gregg, D.R., 1964. Geological Map of New Zealand 1:250,000 Sheet 18 Hurunui, first ed. Department of Scientific and Industrial Research, Wellington.
Griffiths, G.A., McSaveney, M.J., 1983. Distribution of mean annual precipitation across some steepland regions of New Zealand. N. Z. J. Sci. 36, 197–209.
Hales, T.C., Roering, J.J., 2005. Climate-controlled variations in scree production, Southern Alps, New Zealand. Geology 33 (9), 701–704.
Hammer, Ř., Harper, D.A.T., Ryan, P.D., 2001. PAST: paleontological statistics software package for education and data analysis. Palaeontol. Electron. 4 (1), 9 art. 4.
Heiri, O., Lotter, A.F., Lemcke, G., 2001. Loss on ignition as a method for estimating organic and carbonate content in sediments: reproducibility and comparability of results. J. Paleolimnol. 25 (1), 101–110.
Hancock, G.J., Leslie, C., Everett, S.E., Tims, S.G., Brunskill, G.J., Haese, R., 2011. Plutonium as a chronomarker in Australian and New Zealand sediments: a comparison with 137Cs. J. Environ. Radioact. 102, 919–929.
Hilton, R.G., Galy, A., Hovius, N., 2008. Riverine particulate organic carbon from an active mountain belt, importance of landslides. Glob. Biogeochem. Cycles 22, GB1017.
Hogg, A.G., Hua, Q., Blackwell, P.G., Niu, M., Buck, C.E., Guilderson, T.P., Heaton, T.J., Palmer, J.G., Reimer, P.J., Reimer, R.W., Turney, C.S.M., Zimmerman, S.R.H., 2013. SHCal13 southern hemisphere calibration, 0–50,000 Years cal BP. Radiocarbon 55 (4), 1889–1903.
Howarth, J.D., Fitzsimons, S.J., Norris, R.J., Jacobsen, G.E., 2014. Lake sediments record high intensity shaking that provides insight into the location and rupture length of large earthquakes on the Alpine Fault, New Zealand. Earth Planet. Sci. Lett. 403, 340–351.
Howarth, J.D., Fitzsimons, S.J., Norris, R.J., Jacobsen, G.E., Vandergoes, M.J., Norris, R.J., 2013. Identifying a reliable target fraction for radiocarbon dating sedimentary records from lakes. Quat. Geochronol. 17, 68–80.
Howarth, J., Fitzsimons, S.J., Norris, R.J., Langridge, R., Vandergoes, M.J., 2016. A 2000 yr rupture history for the Alpine Fault derived from lake Ellery, South Island, New Zealand. GSA Bull. 2016 (128), 627–643.
Hundey, E.J., Moser, K.A., Longstaffe, F.J., Michelutti, N., Hladyiuk, R., 2014. Recent changes in production in oligotrophic Uinta Mountain lakes, Utah, identified using paleolimnology. Limnol. Oceanogr. 59 (6), 1987–2001.
Jara, I.A., Newnham, R.M., Vandergoes, M.J., Foster, C.R., Lowe, D.J., Wilmshurst, J.M., Moreno, P.I., Renwick, J.A., Homes, A.M., 2015. Pollen–climate reconstruction from northern South Island, New Zealand (41°S), reveals varying high- and low-latitude teleconnections over the last 16 000 years. J. Quat. Sci. 30, 817–829.
Kempema, E.W., Reimnitz, E., Narnes, P.W., 2001. Anchor-ice formation and ice rafting in southwestern Lake Michigan, U.S.A. J. Sediment. Res. 71 (3), 346–354.

Khajavi, N., Langridge, R.M., Quigley, M.C., Smart, C., Rezanejad, A., Martín-González, 2016. Late Holocene rupture behaviour and earthquake chronology on the Hope Fault, New Zealand. Geol. Soc. Am. Bull. 128 (11/12), 1736–1761.
Knuepfer, P.L.K., 1992. Temporal variations in latest quaternary slip across the Australian-Pacific plate boundary, northeastern South Island, New Zealand. Tectonics 11 (3), 449–464.
Koinig, K.A., Kamenik, C., Schmidt, R., Agusti-Panareda, A., Appleby, P., Lami, A., Prazakova, M., Rose, N., Schnell, O.A., Tessadri, R., Thompson, R., Psenner, R., 2002. Environmental changes in an alpine lake (Gossenkollesee, Austria) over the last two centuries the influence of air temperature on biological parameters. J. Paleolimnol. 28 (1), 147–160.
Korup, O., Rixen, C., 2014. Soil erosion and organic carbon export by wet snow avalanches. Cryosphere 8, 651–658.
Langridge, R.M., Almond, P.C., Duncan, R., 2013. Timing of late Holocene paleo-earthquakes on the Hurunui segment of the hope fault: implications for plate boundary strain release through South Island, New Zealand. Geol. Soc. Am. Bull. 125 (5/6), 756–775.
Leathwick, J.R., Wilson, G., Stephens, R.T.T., 2002. Climate Surfaces for New Zealand. Landcare Research Contract Report: LC9798/126. Biodiversity and Conservation Division, Manaaki Whenua — Landcare Research Private Bag 3127, p. 26. Hamilton New Zealand.
Lenzi, M.A., Marchi, L., 2000. Suspended sediment load during floods in a small stream of the Dolomites (northeastern Italy). Catena 39, 267–282.
Leppäranta, M., 2015. Freezing of Lakes and the Evolution of Their Ice Cover. Springer Heidelberg, New York, Dordrecht, London, p. 309.
Liu, X., Colman, S.M., Brown, E.T., Minor, E.C., Li, H., 2013. Estimation of carbonate, total organic carbon, and biogenic silica content by FTIR and XRF techniques in lacustrine sediments. J. Paleolimnol. 50 (3), 387–398.
Lorrey, A., Williams, P., Salinger, J., Martin, T., Palmer, J., Fowler, A., Zhao, J.-X., Neil, H., 2008. Speleothem stable isotope records interpreted within a multi-proxy framework and implications for New Zealand palaeoclimate reconstruction. Quat. Int. 187 (1), 52–75.
Lotter, A.F., Appleby, P.G., Bindler, R., Dearing, J.A., Grytnes, J.A., Hofmann, W., Kamenik, C., Lami, A., Livingstone, D.M., Ohlendorf, C., Rose, N., Sturm, M., 2002. The sediment record of the past 200 years in a Swiss high-alpine lake: Hagelseewli (2339 m a.s.l.). J. Paleolimnol. 28 (1), 111–127.
Luckman, B., 1975. Dropstones resulting from snow-avalanche deposition on lake ice. J. Glaciol. 14 (70), 186–188.
Martel-Cea, A., Maldonado, A., Grosjean, M., Alvial, I., de Jong, R., Fritz, S.C., von Gunten, L., 2016. Late Holocene environmental changes as recorded in the sediments of high Andean Laguna Chepical, Central Chile (32°S; 3050 m a.s.l.). Palaeogeogr. Palaeoclimatol. Palaeoecol. 461, 44–54.
Matsuoka, N., 2001. Direct observation of frost wedging in alpine bedrock. Earth Surf. Process. Landforms 26, 601–614.
McCracken, I.J., 1980. Mountain climate in the Cragieburn range, New Zealand. In: Beneke, U., Davies, M.R. (Eds.), Mountain Environmentas and Subalpine Tree Growth. New Zealand Forest Service, Wellington, New Zealand, pp. 41–59.
National Institute for Water and Atmospheric Research, 2017. The National Climate Database for New Zealand. https://cliflo.niwa.co.nz/. Accessed 7/04/2017.
Nesje, A., Bakke, J., Dahl, S.O., Lie, Ø., Bøe, A.-G., 2007. A continuous, high-resolution 8500-yr snow-avalanche record from western Norway. Holocene 17 (2), 269–277.
New Zealand Earthquake commission, GNS Science. GeoNet Earthquake Catalogue. https://www.geonet.org.nz/data/types/eq_catalogue. Accessed 10th of June 2017.
Robinson, T.R., Davies, T.R.H., Wilson, T.M., Orchiston, C., 2016. Coseismic landsliding estimates for an Alpine Fault earthquake and the consequences for erosion of the Southern Alps, New Zealand. Geomorphology 263, 71–86.
Rodrıguez-Pascua, M.A., Calvo, J.P., De Vicente, G., Gómez-Gras, D., 2000. Soft-sediment deformation structures interpreted as seismites in lacustrine sediments of the Prebetic Zone, SE Spain, and their potential use as indicators of earthquake magnitudes during the Late Miocene. Sediment. Geol. 135 (1–4), 117–135.
Roser, B.P., Korsch, R.J., 1999. Geochemical characterization, evolution and source of a Mesozoic accretionary wedge: the Torlesse terrane, New Zealand. Geol. Mag. 136 (5), 493–512.
Sánchez-López, G., Hernández, A., Pla-Rabes, S., Trigo, R.M., Toro, M., Granados, I., Sáez, A., Masqué, P., Pueyo, J.J., Rubio-Inglés, M.J., Giralt, S., 2016. Climate reconstruction for the last two millennia in central Iberia: the role of East Atlantic (EA), North Atlantic Oscillation (NAO) and their interplay over the Iberian Peninsula. Quat. Sci. Rev. 149, 135–150.
Schindelin, J., Arganda-Carreras, I., Frise, E., Kaynig, V., Longair, M., Pietzsch, T., Preibisch, S., Rueden, C., Saalfeld, S., Schmid, B., Tinevez, J.Y., 2012. Fiji: an open-source platform for biological-image analysis. Nat. Methods 9 (7), 676–682.
Shulmeister, J., McLea, W.L., Singer, C., McKay, Hosie, C., 2003. Late quaternary pollen records from the lower Cobb valley and adjacent areas, North-west Nelson, New Zealand. N. Z. J. Bot. 41, 503–533.
Smith, I.R., 2000. Diamictic sediments within high Arctic lake sediment cores: evidence for lake ice rafting along the lateral glacial margin. Sedimentology 47, 1157–1179.
Spaulding, S.A., McKnight, D.M., Stroermer, E.F., Doran, P.T., 1997. Diatoms in sediments of perennially ice-covered Lake Hoare, and implications for interpreting lake history in the McMurdo Dry Valleys of Antarctica. J. Paleolimnol. 17, 403–420.
Stanley, S., De Deckker, P., 2002. A Holocene record of allochthonous, aeolian mineral grains in an Australian alpine lake; implications for the history of climate change in southeastern Australia. J. Paleolimnol. 27 (2), 207–219.
Stansell, N.D., Rodbell, D.T., Abbott, M.B., Mark, B.G., 2013. Proglacial lake sediment records of Holocene climate change in the western Cordillera of Peru. Quat. Sci. Rev. 70, 1–14.
ter Braak, C.J.F., Šmilauer, P., 2002. CANOCO Reference Manual and CanoDraw for Windows User's Guide: Software for Canonical Community Ordination (Version 4.5) (Microcomputer Power, Ithaca, NY, USA).
Tomkins, J.D., Antoiniades, D., Lamoureux, S.F., Vincent, W.F., 2008. A simple and effective method for preserving the sediment–water interface of sediment cores during transport. J. Paleolimnol. 40 (1), 577–582.
Tomkins, J.D., Lamoureux, S.F., Antoniades, D., Vincent, W.F., 2009. Sedimentary pellets as an ice-cover proxy in a high arctic ice-covered lake. J. Paleolimnol. 41, 225–242.
Vaasma, T., 2008. Grain-size analysis of lacustrine sediments: a comparison of pre-treatment methods. Est. J. Ecol. 57 (4), 231–243.
van der Bilt, W.G.M., Bakke, J., Vasskog, K., D'Andrea, W.J., Bradley, R.S., Ólafsdóttir, S., 2015. Reconstruction of glacier variability from lake sediments reveals dynamic Holocene climate in Svalbard. Quat. Sci. Rev. 126, 201–218.
Vasskog, K., Nesje, A., Støren, E.N., Waldmann, N., Chapron, E., Ariztegui, D., 2011. A Holocene record of snow-avalanche and flood activity reconstructed from a lacustrine sedimentary sequence in Oldevatnet, western Norway. Holocene 21, 597–614.
Wells, A., Yetton, M.D., Duncan, R.P., Stewart, G.H., 1999. Prehistoric dates of the most recent Alpine fault earthquakes, New Zealand. Geology 27 (11), 995–998.
Woller, M.J., Street-Perrott, F.A., Agnew, A.D.Q., 2000. Late quaternary fires and grassland palaeoecology of Mount Kenya, East Africa: evidence from charred grass cuticles in lake sediments. Palaeogeogr. Palaeoclimatol. Palaeoecol. 164 (1–4), 207–230.
Woodward, C., Shulmeister, J., 2006. New Zealand chironomids as proxies for human-induced and natural environmental change: transfer functions for temperature and lake production (chlorophyll a). J. Paleolimnol. 36 (4), 407–429.
Woodward, C., Sloss, C., 2013. Coring and augering. In: Shroder, J.F. (Ed.), Treatise on Geomorphology, Vol. 14. Academic Press, San Diego, pp. 119–137.
Zarnetske, P.L., Hacker, S.D., Seanloom, E.W., Ruggiero, P., Killian, J., Maddux, T.B., Cox, D., 2012. Biophysical feedback mediates effects of invasive grasses on coastal dune shape. Ecology 93, 1439–1450.
Zink, K., Vandergoes, M., Mangelsdorf, K., Dieffenbacher-Krall, A., Schwark, L., 2010. Application of bacterial glycerol dialkyl glycerol tetraethers (GDGTs) to develop modern and past temperature estimates from New Zealand lakes. Org. Geochem. 41, 1060–1066.
Zhou, A., He, Y., Wu, D., Zhang, X., Zhang, C., Liu, Z., Yu, J., 2015. Changes in the radiocarbon reservoir age in lake Xingyun, southwestern China during the Holocene. PLOS one 10 (3), e0121532.